NASA TN D-1015

TECHNICAL NOTE

D-1015

THEORETICAL EVALUATION OF HYPERSONIC FORCES, MOMENTS, AND STABILITY DERIVATIVES FOR COMBINATIONS OF FLAT PLATES, INCLUDING EFFECTS OF BLUNT LEADING EDGES, BY NEWTONIAN IMPACT THEORY

By Walter B. Olstad

Langley Research Center
Langley Air Force Base, Va.

NATIONAL AERONAUTICS AND SPACE ADMINISTRATION
WASHINGTON

March 1962

NATIONAL AERONAUTICS AND SPACE ADMINISTRATION

TECHNICAL NOTE D-1015

THEORETICAL EVALUATION OF HYPERSONIC FORCES, MOMENTS, AND STABILITY DERIVATIVES FOR COMBINATIONS OF FLAT PLATES, INCLUDING EFFECTS OF BLUNT LEADING EDGES, BY NEWTONIAN IMPACT THEORY

By Walter B. Olstad

SUMMARY

A method, based on the modified Newtonian theory, for calculating aerodynamic forces, moments, and stability derivatives at zero sideslip angle for combinations of flat plates of arbitrary planform shape and orientation is presented. Methods for predicting the aerodynamic forces on hemicylindrical leading edges and spherical-wedge nose sections are also presented. Equations are derived and several design-type charts are presented to facilitate computation. Values of the multiplicative factor used in modifying the Newtonian impact theory to account for variations in Mach number and the ratio of specific heats are discussed.

INTRODUCTION

Newtonian impact theory as modified according to Lees (ref. 1), where the empirical modification consists of a multiplicative factor which makes the formula for the pressure coefficient give the correct stagnation pressure, has proven extremely useful in the prediction of static forces and moments on bodies at hypersonic speeds. Simplified methods of application to the steady-state case of the modified theory without the Busemann centrifugal correction for arbitrary inclined bodies of revolution are presented in references 2 and 3. An extension of these Newtonian concepts without the centrifugal correction to the quasi-steady case has been applied to determine the stability derivatives of bodies of revolution in references 4, 5, and 6. The use of a quasi-steady approach for the determination of stability derivatives rather than the use of an unsteady flow theory, such as that developed by Hayes and Probstein (ref. 7), may be justified by the fact that the reduced frequency of the motion of the body is very much smaller than unity at the free-stream velocities of interest.

The purpose of this analysis is to present a method, based on the modified Newtonian theory, for calculating the aerodynamic forces, moments, and stability derivatives for combinations of flat plates of arbitrary planform shape and orientation. Because the reduced frequency of motion of these surfaces is very small compared with unity, the quasi-steady approach is used and the centrifugal correction is neglected. (The fluid particles actually follow an accelerated or curved path in the case of an oscillating flat plate, the amount of curvature depending on the reduced frequency of oscillation.) Methods for predicting the aerodynamic forces on hemicylindrical leading edges and spherical-wedge nose sections are also presented. The centrifugal correction is also neglected in the derivation of force and moment expressions for the leading edges and noses, because the modified Newtonian impact theory without this correction has been shown to be in better agreement with experiment (for example, ref. 8) than the theory with the centrifugal correction.

Application of the present method to a specific configuration is presented and values of the multiplicative factor used in modifying the Newtonian impact theory to account for variations in Mach number and the ratio of specific heats are discussed.

SYMBOLS

a, b, c distances in x-, y-, and z-directions, respectively, from the origin of the body-axis system to the centroid of area of the deflected surface

a', b', c' distances in x-, y-, and z-directions, respectively, from an arbitrary moment reference center (1) to a second moment reference center (2)

A_1, A_2 functions for evaluation of axial-force coefficient on hemicylindrical leading edge

C_A axial-force coefficient, $\dfrac{\text{Axial force}}{q_\infty S}$

C_l rolling-moment coefficient, $\dfrac{\text{Rolling moment}}{q_\infty S l}$

C_m pitching-moment coefficient, $\dfrac{\text{Pitching moment}}{q_\infty S l}$

C_N normal-force coefficient, $\dfrac{\text{Normal force}}{q_\infty S}$

C_n yawing-moment coefficient, $\frac{\text{Yawing moment}}{q_\infty S l}$

C_p pressure coefficient, $\frac{p_L - p_\infty}{q_\infty}$

C_Y side-force coefficient, $\frac{\text{Side force}}{q_\infty S}$

$f_1(\xi), f_2(\xi), f_3(\xi), f_4(\xi)$ functions for evaluation of force coefficients on hemicylindrical leading edge

$\bar{I}_X$ moment of inertia of deflected surface with respect to an axis parallel to the x'-axis and passing through the centroid of area of the surface

$\bar{I}_Y$ moment of inertia of deflected surface with respect to an axis parallel to the y'-axis and passing through the centroid of area of the surface

$\bar{I}_{XY}$ product of inertia of the deflected surface with respect to a pair of axes parallel to the x' and y' axes and passing through the centroid of area of the surface

$\vec{i}, \vec{j}, \vec{k}$ unit vectors in the body-axis system

K multiplicative factor in the Newtonian expression for the pressure coefficient (see eq. (6))

l reference length

L length of square-cut section of hemicylindrical leading edge (fig. 9)

M_∞ free-stream Mach number

$\vec{n}$ unit vector normal to deflected surface, positive in direction of Z'-axis

N_1, N_2 functions for evaluation of normal-force coefficient on hemicylindrical leading edge

p, q, r angular velocities of the deflected surface about the body-axis system

p_L	local static pressure
p_∞	free-stream static pressure
q_∞	free-stream dynamic pressure, $\frac{\gamma}{2} p_\infty M_\infty^2$
$\vec{r}$	unit radius vector of hemicylindrical leading edge (fig. 9) or of spherical-wedge nose section (fig. 11), positive when pointed out of surface
R	radius of hemicylindrical leading edge (fig. 9) or of spherical-wedge nose section (fig. 11)
S	reference area
U	distance along hemicylindrical leading edge
$\vec{U}$	unit vector parallel to hemicylindrical leading edge
U_X, U_Y, U_Z	scalar components of vector $\vec{U}$ in the x-, y-, and z-directions, respectively
V_N	velocity normal to deflected surface; arrow over symbol indicates vector
$\vec{V}_{N,s}$	normal velocity vector at the stagnation line of a hemicylindrical leading edge
V_∞	free-stream velocity; arrow over symbol indicates vector
X, Y, Z	body axes
x, y, z	coordinates in body-axis system (see fig. 1)
X', Y', Z'	axes of deflected surface after rotation through angles Γ, δ, and ϵ (see fig. 2)
x', y', z'	coordinates in X', Y', and Z' system of axes
$\bar{x}, \bar{y}, \bar{z}$	distances in x-, y-, and z-directions, respectively, of a point on the deflected surface from the centroid of area of the surface

$\bar{x}', \bar{y}', \bar{z}'$	distances in x'-, y'-, and z'-directions, respectively, of a point on the deflected surface from the centroid of area of the surface
Y_1, Y_2	functions for evaluation of side-force ceofficient on hemicylindrical leading edge
α	angle of attack (see fig. 1)
β	angle of sideslip (see fig. 1)
γ	isentropic exponent (equal to ratio of specific heats for a perfect gas)
γ_e	effective value of γ, including effects of ionization and dissociation
Γ, δ, ϵ	surface orientation angles in preferred order of rotation (see fig. 2)
η	angle between the free stream and unit vector normal to surface
θ	angle defined by figure 9(c)
Λ	angle of sweepback of leading edge (fig. 9)
Λ_e	effective angle of sweepback of leading edge (eq. (A3))
λ	angle defined by figure 9(e)
ξ	angle defined by figure 9(c)
$\vec{\rho}$	radius vector from the center of rotation to a point on the deflected surface, defined by equation (5)
ρ	density behind oblique shock
ρ_∞	density in free stream
σ	angle between oblique shock and free-stream direction
τ	angle defined by figure 9(d)
Φ, Ψ	functions for evaluation of normal- and axial-force coefficients on a spherical-wedge nose section
ϕ	angle defined by figure 11

ϕ_o limiting value of ϕ defined by equation (B6)

ψ angle defined by figure 11

ψ_o limiting value of ψ defined by equation (B9)

$\vec{\omega}$ angular velocity vector, defined by equation (4)

Superscript:

. time derivative

Subscripts:

i ith component

l position 1 for moment reference center

2 position 2 for moment reference center

T equilibrium or trim value

tot total

s stagnation point

When α, β, p, q, and r are used as subscripts, a dimensionless derivative is indicated as defined by equations (12).

ANALYSIS

For this analysis, the undeflected surface of a flat plate of arbitrary planform is considered to lie in the xy-plane of the body-axis system. Positive directions of distances, flow-direction angles, and rotational velocities in this system are illustrated in figure 1. The deflected surface lies in a transformed plane with the axes oriented through the angles Γ, δ, and ϵ (in that order), as illustrated in figure 2. For an arbitrarily deflected flat surface, which lies in the xy-plane of the body-axis system, rotating about a point with an angular velocity $\vec{\omega}$ (fig. 3) the magnitude of the normal velocity vector $\vec{V}_N$ at a distance $\vec{\rho}$ from the center of rotation is given as

$$V_N = -\vec{n}\cdot\vec{V}_\infty + \vec{n}\cdot(\vec{\omega}\times\vec{\rho}) \qquad (1)$$

(It is shown in reference 4, that the impact theory, when applied to a uniformly accelerating motion, gives zero for the force and moment proportional to the accelerating parameter (that is, $\dot{\alpha}l/V_\infty$ and $\dot{\beta}l/V_\infty$).)

In equation (1), the term $\vec{n}$ is the unit normal vector of the deflected surface and can be represented in terms of the body-axis system as follows:

$$\vec{n} = \vec{i} \sin \delta - \vec{j} \sin \Gamma \cos \delta + \vec{k} \cos \Gamma \cos \delta \tag{2}$$

The free-stream velocity vector $\vec{V}_\infty$ is

$$\vec{V}_\infty = V_\infty(-\vec{i} \cos \alpha \cos \beta - \vec{j} \sin \beta - \vec{k} \sin \alpha \cos \beta) \tag{3}$$

The angular velocity vector $\vec{\omega}$ is

$$\vec{\omega} = \vec{i}p + \vec{j}q + \vec{k}r \tag{4}$$

and the vector $\vec{\rho}$ is given by

$$\vec{\rho} = \vec{i}x + \vec{j}y + \vec{k}z \tag{5}$$

The pressure coefficient for the modified Newtonian impact theory can be expressed as

$$C_p = \frac{p_L - p_\infty}{q_\infty} = K\left(\frac{V_N}{V_\infty}\right)^2 \tag{6}$$

It is to be noted that equation (6) is applicable only to those surface areas that face the flow; for surface areas that are shielded from the flow it is assumed that $C_p = 0$. The condition that the surface "see" the flow may be expressed as $\frac{\pi}{2} \leqq \eta \leqq \frac{3\pi}{2}$, where η is the angle between the free-stream velocity vector and the unit vector normal to the surface (fig. 3). Thus,

$$\cos \eta = - \frac{\vec{n} \cdot \vec{V}_\infty}{V_\infty} \tag{7}$$

and the condition that the surface see the flow may also be expressed as $\cos \eta \leqq 0$.

The pressure coefficient can be written, from equations (1) to (6), as

$$C_p = K\left\{\cos^2\eta + 2\cos\eta\left[\left(\vec{n}\cdot\vec{i}\right)\left(\frac{qz - ry}{V_\infty}\right) - \left(\vec{n}\cdot\vec{j}\right)\left(\frac{pz - rx}{V_\infty}\right) + \left(\vec{n}\cdot\vec{k}\right)\left(\frac{py - qx}{V_\infty}\right)\right]\right.$$

$$\left. + \left[\left(\vec{n}\cdot\vec{i}\right)\left(\frac{qz - ry}{V_\infty}\right) - \left(\vec{n}\cdot\vec{j}\right)\left(\frac{pz - rx}{V_\infty}\right) + \left(\vec{n}\cdot\vec{k}\right)\left(\frac{py - qx}{V_\infty}\right)\right]^2\right\} \tag{8}$$

The force and moment coefficients based on the area of the deflected surface and on some characteristic length l are,

$$C_N = \frac{1}{S}\iint_S C_p\,\vec{k}\cdot\vec{n}\,dS \tag{9a}$$

$$C_A = \frac{1}{S}\iint_S C_p\,\vec{i}\cdot\vec{n}\,dS \tag{9b}$$

$$C_Y = -\frac{1}{S}\iint_S C_p\,\vec{j}\cdot\vec{n}\,dS \tag{9c}$$

$$C_m = \frac{1}{Sl}\iint_S xC_p\vec{k}\cdot\vec{n}\,dS - \frac{1}{Sl}\iint_S zC_p\vec{i}\cdot\vec{n}\,dS \tag{9d}$$

$$C_l = -\frac{1}{Sl}\iint_S yC_p\vec{k}\cdot\vec{n}\,dS + \frac{1}{Sl}\iint_S zC_p\vec{j}\cdot\vec{n}\,dS \tag{9e}$$

$$C_n = -\frac{1}{Sl}\iint_S xC_p\vec{j}\cdot\vec{n}\,dS + \frac{1}{Sl}\iint_S yC_p\vec{i}\cdot\vec{n}\,dS \tag{9f}$$

In a stability analysis, small deviations from some equilibrium condition are usually of interest. These deviations may be represented in equations (9) by letting the flow-direction angles be

$$\left.\begin{aligned}\alpha &= \alpha_T + \Delta\alpha\\ \beta &= \beta_T + \Delta\beta\end{aligned}\right\} \tag{10}$$

where the subscript T indicates the angle corresponding to the equilibrium (trim) condition and the Δ-quantities are small deviations in these angles.

At the extreme flight velocities for which this analysis applies, the rotational velocity parameters pl/V_∞, ql/V_∞, and rl/V_∞ would be very much less than unity. The results of an analog study in reference 9 indicate that values of ql/V_∞ for vehicles considered as typical for reentry or hypervelocity flight are on the order of 0.01. Thus, for the remainder of this analysis values of the rotational velocity parameters are assumed to approach zero.

The force and moment coefficients may now be written

$$\left.\begin{aligned} C_N &= C_N(\alpha_T, \beta_T) + \Delta C_N \\ C_A &= C_A(\alpha_T, \beta_T) + \Delta C_A \\ C_Y &= C_Y(\alpha_T, \beta_T) + \Delta C_Y \\ C_m &= C_m(\alpha_T, \beta_T) + \Delta C_m \\ C_l &= C_l(\alpha_T, \beta_T) + \Delta C_l \\ C_n &= C_n(\alpha_T, \beta_T) + \Delta C_n \end{aligned}\right\} \tag{11}$$

Since the quantities $\Delta\alpha$ and $\Delta\beta$ are small, use of the small-angle approximation is permissible. Hence, retaining only first-order terms in these quantities yields, for the derivatives of interest in stability analyses:

$$C_{N_\alpha} = \left(\frac{\partial C_N}{\partial \Delta\alpha}\right)_{\Delta\alpha\to 0} = \frac{1}{S} \iint_S \left(\frac{\partial C_p}{\partial \Delta\alpha}\right)_{\Delta\alpha\to 0} \vec{k}\cdot\vec{n}\, dS \tag{12a}$$

$$C_{A_\alpha} = \left(\frac{\partial C_A}{\partial \Delta\alpha}\right)_{\Delta\alpha\to 0} = \frac{1}{S} \iint_S \left(\frac{\partial C_p}{\partial \Delta\alpha}\right)_{\Delta\alpha\to 0} \vec{i}\cdot\vec{n}\, dS \tag{12b}$$

$$C_{m_\alpha} = \left(\frac{\partial C_m}{\partial \Delta\alpha}\right)_{\Delta\alpha\to 0} = \frac{1}{Sl} \iint_S x\left(\frac{\partial C_p}{\partial \Delta\alpha}\right)_{\Delta\alpha\to 0} \vec{k}\cdot\vec{n}\, dS - \frac{1}{Sl} \iint_S z\left(\frac{\partial C_p}{\partial \Delta\alpha}\right)_{\Delta\alpha\to 0} \vec{i}\cdot\vec{n}\, dS \tag{12c}$$

$$C_{N_q} = \left(\frac{\partial C_N}{\partial \frac{ql}{V_\infty}}\right)_{q\to 0} = \frac{1}{S} \iint_S \left(\frac{\partial C_p}{\partial \frac{ql}{V_\infty}}\right)_{q\to 0} \vec{k}\cdot\vec{n}\, dS \tag{12d}$$

$$C_{A_q} = \left(\frac{\partial C_A}{\partial \frac{ql}{V_\infty}}\right)_{q\to 0} = \frac{1}{S} \iint_S \left(\frac{\partial C_p}{\partial \frac{ql}{V_\infty}}\right)_{q\to 0} \vec{i}\cdot\vec{n}\, dS \tag{12e}$$

L
1
6
9
1

$$C_{m_q} = \left(\frac{\partial C_m}{\partial \frac{ql}{V_\infty}}\right)_{q\to 0}$$

$$= \frac{1}{Sl} \iint_S x\left(\frac{\partial C_p}{\partial \frac{ql}{V_\infty}}\right)_{q\to 0} \vec{k}\cdot\vec{n}\, dS - \frac{1}{Sl} \iint_S z\left(\frac{\partial C_p}{\partial \frac{ql}{V_\infty}}\right)_{q\to 0} \vec{i}\cdot\vec{n}\, dS \tag{12f}$$

$$C_{Y_\beta} = \left(\frac{\partial C_Y}{\partial \Delta\beta}\right)_{\Delta\beta\to 0} = -\frac{1}{S} \iint_S \left(\frac{\partial C_p}{\partial \Delta\beta}\right)_{\Delta\beta\to 0} \vec{j}\cdot\vec{n}\, dS \tag{12g}$$

$$C_{n_\beta} = \left(\frac{\partial C_n}{\partial \Delta\beta}\right)_{\Delta\beta\to 0}$$

$$= -\frac{1}{Sl} \iint_S x\left(\frac{\partial C_p}{\partial \Delta\beta}\right)_{\Delta\beta\to 0} \vec{j}\cdot\vec{n}\, dS + \frac{1}{Sl} \iint_S y\left(\frac{\partial C_p}{\partial \Delta\beta}\right)_{\Delta\beta\to 0} \vec{i}\cdot\vec{n}\, dS \tag{12h}$$

$$C_{l_\beta} = \left(\frac{\partial C_l}{\partial \Delta\beta}\right)_{\Delta\beta\to 0}$$

$$= -\frac{1}{Sl} \iint_S y\left(\frac{\partial C_p}{\partial \Delta\beta}\right)_{\Delta\beta\to 0} \vec{k}\cdot\vec{n}\, dS + \frac{1}{Sl} \iint_S z\left(\frac{\partial C_p}{\partial \Delta\beta}\right)_{\Delta\beta\to 0} \vec{j}\cdot\vec{n}\, dS \tag{12i}$$

$$C_{n_p} = \left(\frac{\partial C_n}{\partial \frac{pl}{V_\infty}}\right)_{p\to 0}$$

$$= -\frac{1}{Sl}\iint_S x\left(\frac{\partial C_p}{\partial \frac{pl}{V_\infty}}\right)_{p\to 0} \vec{j}\cdot\vec{n}\, dS + \frac{1}{Sl}\iint_S y\left(\frac{\partial C_p}{\partial \frac{pl}{V_\infty}}\right)_{p\to 0} \vec{i}\cdot\vec{n}\, dS \qquad (12j)$$

$$C_{l_p} = \left(\frac{\partial C_l}{\partial \frac{pl}{V_\infty}}\right)_{p\to 0}$$

$$= -\frac{1}{Sl}\iint_S y\left(\frac{\partial C_p}{\partial \frac{pl}{V_\infty}}\right)_{p\to 0} \vec{k}\cdot\vec{n}\, dS + \frac{1}{Sl}\iint_S z\left(\frac{\partial C_p}{\partial \frac{pl}{V_\infty}}\right)_{p\to 0} \vec{j}\cdot\vec{n}\, dS \qquad (12k)$$

$$C_{n_r} = \left(\frac{\partial C_n}{\partial \frac{rl}{V_\infty}}\right)_{r\to 0}$$

$$= -\frac{1}{Sl}\iint_S x\left(\frac{\partial C_p}{\partial \frac{rl}{V_\infty}}\right)_{r\to 0} \vec{j}\cdot\vec{n}\, dS + \frac{1}{Sl}\iint_S y\left(\frac{\partial C_p}{\partial \frac{rl}{V_\infty}}\right)_{r\to 0} \vec{i}\cdot\vec{n}\, dS \qquad (12l)$$

$$C_{l_r} = \left(\frac{\partial C_l}{\partial \frac{rl}{V_\infty}}\right)_{r\to 0}$$

$$= -\frac{1}{Sl}\iint_S y\left(\frac{\partial C_p}{\partial \frac{rl}{V_\infty}}\right)_{r\to 0} \vec{k}\cdot\vec{n}\, dS + \frac{1}{Sl}\iint_S z\left(\frac{\partial C_p}{\partial \frac{rl}{V_\infty}}\right)_{r\to 0} \vec{j}\cdot\vec{n}\, dS \qquad (12m)$$

In most analyses the trim value of the sideslip angle β is considered to be zero. This assumption shall be used hereinafter. The pressure coefficient and the various derivatives under the foregoing assumptions for the flow-direction angles and the rotational velocities become

$$\left.\begin{aligned}
C_p &= K \cos^2\eta \\
\left(\frac{\partial C_p}{\partial \Delta\alpha}\right)_{\Delta\alpha\to 0} &= 2K \cos\eta \left(\frac{d}{d\Delta\alpha} \cos\eta\right)_{\Delta\alpha\to 0} \\
\left(\frac{\partial C_p}{\partial \Delta\beta}\right)_{\Delta\beta\to 0} &= 2K \cos\eta \left(\frac{d}{d\Delta\beta} \cos\eta\right)_{\Delta\beta\to 0} \\
\left(\frac{\partial C_p}{\partial \frac{pl}{V_\infty}}\right)_{p\to 0} &= 2K \cos\eta \left[-(\vec{n}\cdot\vec{j})\left(\frac{z}{l}\right) + (\vec{n}\cdot\vec{k})\left(\frac{y}{l}\right)\right] \\
\left(\frac{\partial C_p}{\partial \frac{ql}{V_\infty}}\right)_{q\to 0} &= 2K \cos\eta \left[(\vec{n}\cdot\vec{i})\left(\frac{z}{l}\right) - (\vec{n}\cdot\vec{k})\left(\frac{x}{l}\right)\right] \\
\left(\frac{\partial C_p}{\partial \frac{rl}{V_\infty}}\right)_{r\to 0} &= 2K \cos\eta \left[-(\vec{n}\cdot\vec{i})\left(\frac{y}{l}\right) + (\vec{n}\cdot\vec{j})\left(\frac{x}{l}\right)\right]
\end{aligned}\right\} \qquad (13)$$

The various scalar products in the expressions (12) and (13) may be written:

$$\left.\begin{aligned}
\vec{n}\cdot\vec{i} &= \sin\delta \\
\vec{n}\cdot\vec{j} &= -\sin\Gamma\cos\delta \\
\vec{n}\cdot\vec{k} &= \cos\Gamma\cos\delta
\end{aligned}\right\} \qquad (14)$$

Substituting equations (2) and (3) into equation (7) yields the following expression for $\cos\eta$:

$$\cos\eta = -\cos\alpha\cos\beta\sin\delta - \sin\beta\sin\Gamma\cos\delta + \sin\alpha\cos\beta\cos\Gamma\cos\delta \qquad (15)$$

L 1 6 9 1

and

$$\left.\begin{aligned}\frac{d}{d\Delta\alpha}(\cos\eta) &= -\sin\alpha\sin\delta + \cos\alpha\cos\Gamma\cos\delta \\ \frac{d}{d\Delta\beta}(\cos\eta) &= -\sin\Gamma\cos\delta\end{aligned}\right\} \tag{16}$$

Substituting equations (13), (14), and (16) into equations (9) and (12) yields the following expressions for the coefficients and derivatives of interest:

$$C_N = K\cos^2\eta\cos\Gamma\cos\delta \tag{17a}$$

$$C_A = K\cos^2\eta\sin\delta \tag{17b}$$

$$C_Y = K\cos^2\eta\sin\Gamma\cos\delta \tag{17c}$$

$$C_l = -K\cos^2\eta\left(\cos\Gamma\cos\delta\iint_S\frac{y}{l}\frac{dS}{S} + \sin\Gamma\cos\delta\iint_S\frac{z}{l}\frac{dS}{S}\right) \tag{17d}$$

$$C_m = K\cos^2\eta\left(\cos\Gamma\cos\delta\iint_S\frac{x}{l}\frac{dS}{S} - \sin\delta\iint_S\frac{z}{l}\frac{dS}{S}\right) \tag{17e}$$

$$C_n = K\cos^2\eta\left(\sin\Gamma\cos\delta\iint_S\frac{x}{l}\frac{dS}{S} + \sin\delta\iint_S\frac{y}{l}\frac{dS}{S}\right) \tag{17f}$$

$$C_{N_\alpha} = 2K\cos\eta\left[\frac{\partial}{\partial\Delta\alpha}(\cos\eta)\right]\cos\Gamma\cos\delta \tag{17g}$$

$$C_{A_\alpha} = 2K\cos\eta\left[\frac{\partial}{\partial\Delta\alpha}(\cos\eta)\right]\sin\delta \tag{17h}$$

$$C_{m_\alpha} = 2K\cos\eta\left[\frac{\partial}{\partial\Delta\alpha}(\cos\eta)\right]\left(\cos\Gamma\cos\delta\iint_S\frac{x}{l}\frac{dS}{S} - \sin\delta\iint_S\frac{z}{l}\frac{dS}{S}\right) \tag{17i}$$

$$C_{N_q} = -2K\cos\eta\cos\Gamma\cos\delta\left(\cos\Gamma\cos\delta\iint_S\frac{x}{l}\frac{dS}{S} - \sin\delta\iint_S\frac{z}{l}\frac{dS}{S}\right) \tag{17j}$$

$$C_{A_q} = -2K \cos \eta \sin \delta \left(\cos \Gamma \cos \delta \iint_S \frac{x}{l} \frac{dS}{S} - \sin \delta \iint_S \frac{z}{l} \frac{dS}{S} \right) \quad (17k)$$

$$C_{m_q} = -2K \cos \eta \left(\cos^2 \Gamma \cos^2 \delta \iint_S \frac{x^2}{l^2} \frac{dS}{S} - 2 \cos \Gamma \sin \delta \cos \delta \iint_S \frac{xz}{l^2} \frac{dS}{S} \right.$$

$$\left. + \sin^2 \delta \iint_S \frac{z^2}{l^2} \frac{dS}{S} \right) \quad (17l)$$

$$C_{Y_\beta} = -2K \cos \eta \sin^2 \Gamma \cos^2 \delta \quad (17m)$$

$$C_{n_\beta} = -2K \cos \eta \cos \delta \left(\sin \Gamma \cos \delta \iint_S \frac{x}{l} \frac{dS}{S} + \sin \delta \iint_S \frac{y}{l} \frac{dS}{S} \right) \quad (17n)$$

$$C_{l_\beta} = 2K \cos \eta \sin \Gamma \cos \delta \left(\cos \Gamma \cos \delta \iint_S \frac{y}{l} \frac{dS}{S} + \sin \Gamma \cos \delta \iint_S \frac{z}{l} \frac{dS}{S} \right) \quad (17o)$$

$$C_{n_p} = 2K \cos \eta \cos \delta \left[\sin \Gamma \left(\cos \Gamma \cos \delta \iint_S \frac{xy}{l^2} \frac{dS}{S} + \sin \delta \iint_S \frac{yz}{l^2} \frac{dS}{S} \right. \right.$$

$$\left. \left. + \sin \Gamma \cos \delta \iint_S \frac{zx}{l^2} \frac{dS}{S} \right) + \cos \Gamma \sin \delta \iint_S \frac{y^2}{l^2} \frac{dS}{S} \right] \quad (17p)$$

$$C_{l_p} = -2K \cos \eta \cos^2 \delta \left(\cos^2 \Gamma \iint_S \frac{y^2}{l^2} \frac{dS}{S} + 2 \sin \Gamma \cos \Gamma \iint_S \frac{yz}{l^2} \frac{dS}{S} \right.$$

$$\left. + \sin^2 \Gamma \iint_S \frac{z^2}{l^2} \frac{dS}{S} \right) \quad (17q)$$

$$C_{n_r} = -2K \cos \eta \left(\sin^2 \Gamma \cos^2 \delta \iint_S \frac{x^2}{l^2} \frac{dS}{S} + 2 \sin \Gamma \sin \delta \cos \delta \iint_S \frac{xy}{l^2} \frac{dS}{S} \right.$$

$$\left. + \sin^2 \delta \iint_S \frac{y^2}{l^2} \frac{dS}{S} \right) \tag{17r}$$

$$C_{l_r} = 2K \cos \eta \cos \delta \left[\sin \Gamma \left(\cos \Gamma \cos \delta \iint_S \frac{xy}{l^2} \frac{dS}{S} + \sin \delta \iint_S \frac{yz}{l^2} \frac{dS}{S} \right.\right.$$

$$\left.\left. + \sin \Gamma \cos \delta \iint_S \frac{zx}{l^2} \frac{dS}{S} \right) + \cos \Gamma \sin \delta \iint_S \frac{y^2}{l^2} \frac{dS}{S} \right] \tag{17s}$$

L
1
6
9
1

Curves of $\cos \eta$ and $\frac{\partial}{\partial \Delta\alpha}(\cos \eta)$ as functions of angle of attack and of the surface orientation angles Γ and δ for zero sideslip angle (eqs. (15) and (16), are presented in figures 4 and 5, respectively.

If the body-axis system (x, y, and z) is transferred to the centroid of area of the deflected surface, the original distances become

$$\left.\begin{aligned} x &= \bar{x} + a \\ y &= \bar{y} + b \\ z &= \bar{z} + c \end{aligned}\right\} \tag{18}$$

where $\bar{x}$, $\bar{y}$, and $\bar{z}$ are the distances in the x-, y-, and z-directions, respectively, of a point on the deflected surface from the centroid of area of the surface, and where a, b, and c are the distances in the x-, y-, and z-directions, respectively, from the origin of the body-axis system to the centroid of area of the deflected surface. Writing the $\bar{x}$-, $\bar{y}$-, and $\bar{z}$-distances in terms of the coordinate system of the deflected surface ($\bar{x}'$, $\bar{y}'$, $\bar{z}'$) yields

$$\left.\begin{aligned} \bar{x} &= \bar{x}' \cos \delta \cos \epsilon - \bar{y}' \cos \delta \sin \epsilon \\ \bar{y} &= \bar{x}'(\sin \Gamma \sin \delta \cos \epsilon + \cos \Gamma \sin \epsilon) \\ &\quad + \bar{y}'(\cos \Gamma \cos \epsilon - \sin \Gamma \sin \delta \sin \epsilon) \\ \bar{z} &= \bar{x}'(\sin \Gamma \sin \epsilon - \cos \Gamma \sin \delta \cos \epsilon) \\ &\quad + \bar{y}'(\sin \Gamma \cos \epsilon + \cos \Gamma \sin \delta \sin \epsilon) \end{aligned}\right\} \tag{19}$$

Thus, the integrals of equations (17) when expressed in terms of the surface coordinate system and the transfer distances a, b, and c become:

$$\iint_S \left(\frac{x}{l}\right)\frac{dS}{S} = \frac{a}{l} \tag{20a}$$

$$\iint_S \left(\frac{y}{l}\right)\frac{dS}{S} = \frac{b}{l} \tag{20b}$$

$$\iint_S \left(\frac{z}{l}\right)\frac{dS}{S} = \frac{c}{l} \tag{20c}$$

$$\iint_S \left(\frac{x}{l}\right)^2 \frac{dS}{S} = \left[\frac{\bar{I}_Y}{Sl^2}\cos^2\epsilon + \frac{\bar{I}_X}{Sl^2}\sin^2\epsilon\right]\cos^2\delta - 2\frac{\bar{I}_{XY}}{Sl^2}\sin\epsilon\cos\epsilon\cos^2\delta + \left(\frac{a}{l}\right)^2 \tag{20d}$$

$$\iint_S \left(\frac{y}{l}\right)^2 \frac{dS}{S} = \left[\frac{\bar{I}_Y}{Sl^2}(\sin\Gamma\sin\delta\cos\epsilon + \cos\Gamma\sin\epsilon)^2 + \frac{\bar{I}_X}{Sl^2}(\cos\Gamma\cos\epsilon - \sin\Gamma\sin\delta\sin\epsilon)^2\right] + 2\frac{\bar{I}_{XY}}{Sl^2}(\sin\Gamma\sin\delta\cos\epsilon + \cos\Gamma\sin\epsilon)(\cos\Gamma\cos\epsilon - \sin\Gamma\sin\delta\sin\epsilon) + \left(\frac{b}{l}\right)^2 \tag{20e}$$

$$\iint_S \left(\frac{z}{l}\right)^2 \frac{dS}{S} = \frac{\bar{I}_Y}{Sl^2}(\sin\Gamma\sin\epsilon - \cos\Gamma\sin\delta\cos\epsilon)^2 + \frac{\bar{I}_X}{Sl^2}(\sin\Gamma\cos\epsilon + \cos\Gamma\sin\delta\sin\epsilon)^2 + 2\frac{\bar{I}_{XY}}{Sl^2}(\sin\Gamma\sin\epsilon - \cos\Gamma\sin\delta\cos\epsilon)(\sin\Gamma\cos\epsilon + \cos\Gamma\sin\delta\sin\epsilon) + \left(\frac{c}{l}\right)^2 \tag{20f}$$

$$\iint_S \left(\frac{xy}{l^2}\right)\frac{dS}{S} = \frac{\bar{I}_Y}{Sl^2}\cos\delta\cos\epsilon(\sin\Gamma\sin\delta\cos\epsilon + \cos\Gamma\sin\epsilon)$$

$$- \frac{\bar{I}_X}{Sl^2}\cos\delta\sin\epsilon(\cos\Gamma\cos\epsilon - \sin\Gamma\sin\delta\sin\epsilon)$$

$$+ \frac{\bar{I}_{XY}}{Sl^2}\Big[\cos\delta\cos\epsilon(\cos\Gamma\cos\epsilon - \sin\Gamma\sin\delta\sin\epsilon)$$

$$- \cos\delta\sin\epsilon(\sin\Gamma\sin\delta\cos\epsilon + \cos\Gamma\sin\epsilon)\Big] + \frac{ab}{l^2} \qquad (20g)$$

$$\iint_S \left(\frac{yz}{l^2}\right)\frac{dS}{S} = \frac{\bar{I}_Y}{Sl^2}(\sin\Gamma\sin\delta\cos\epsilon + \cos\Gamma\sin\epsilon)(\sin\Gamma\sin\epsilon$$

$$- \cos\Gamma\sin\delta\cos\epsilon) + \frac{\bar{I}_Y}{Sl^2}(\cos\Gamma\cos\epsilon$$

$$- \sin\Gamma\sin\delta\sin\epsilon)(\sin\Gamma\cos\epsilon + \cos\Gamma\sin\delta\sin\epsilon)$$

$$+ \frac{\bar{I}_{XY}}{Sl^2}\Big[(\sin\Gamma\sin\delta\cos\epsilon + \cos\Gamma\sin\epsilon)(\sin\Gamma\cos\epsilon$$

$$+ \cos\Gamma\sin\delta\sin\epsilon) + (\cos\Gamma\cos\epsilon$$

$$- \sin\Gamma\sin\delta\sin\epsilon)(\sin\Gamma\sin\epsilon - \cos\Gamma\sin\delta\cos\epsilon)\Big] + \frac{bc}{l^2} \qquad (20h)$$

L
1
6
9
1

$$\iint_S \left(\frac{zx}{l^2}\right)\frac{dS}{S} = \frac{\bar{I}_Y}{Sl^2}\cos\delta\cos\epsilon(\sin\Gamma\sin\epsilon - \cos\Gamma\sin\delta\cos\epsilon)$$

$$- \frac{\bar{I}_X}{Sl^2}\cos\delta\sin\epsilon(\sin\Gamma\cos\epsilon + \cos\Gamma\sin\delta\sin\epsilon)$$

$$+ \frac{\bar{I}_{XY}}{Sl^2}\left[\cos\delta\cos\epsilon(\sin\Gamma\cos\epsilon + \cos\Gamma\sin\delta\sin\epsilon)\right.$$

$$\left. - \cos\delta\sin\epsilon(\sin\Gamma\sin\epsilon - \cos\Gamma\sin\delta\cos\epsilon)\right] + \frac{ac}{l^2} \qquad (20i)$$

L 1691

where $\bar{I}_X$ and $\bar{I}_Y$ are the moments of inertia of the deflected surface about axes parallel to the X' and Y' axes and passing through the centroid of area of the surface, respectively, and $\bar{I}_{XY}$ is the product of inertia of the deflected surface with respect to a pair of axes parallel to the X' and Y' axes and passing through the centroid of area of the surface.

A change in the location of the moment reference center may be effected by means of the following relations:

$$C_{m_2} = C_{m_1} + C_{N_1}\frac{a'}{l} - C_{A_1}\frac{c'}{l} \qquad (21a)$$

$$C_{n_2} = C_{n_1} + C_{Y_1}\frac{a'}{l} + C_{A_1}\frac{b'}{l} \qquad (21b)$$

$$C_{l_2} = C_{l_1} - C_{N_1}\frac{b'}{l} - C_{Y_1}\frac{c'}{l} \qquad (21c)$$

$$C_{m_{\alpha_2}} = C_{m_{\alpha_1}} + C_{N_{\alpha_1}}\frac{a'}{l} - C_{A_{\alpha_1}}\frac{c'}{l} \qquad (21d)$$

$$C_{N_{q_2}} = C_{N_{q_1}} + 2K\cos\eta\cos\Gamma\cos\delta\left(\sin\delta\frac{c'}{l} - \cos\Gamma\cos\delta\frac{a'}{l}\right) \qquad (21e)$$

$$C_{A_{q_2}} = C_{A_{q_1}} + 2K\cos\eta\sin\delta\left(\sin\delta\frac{c'}{l} - \cos\Gamma\cos\delta\frac{a'}{l}\right) \qquad (21f)$$

$$C_{m_{q_2}} = C_{m_{q_1}} - 2K \cos \eta \left[\cos^2\Gamma \cos^2\delta \left(\frac{a'}{l}\right)^2 - 2 \cos \Gamma \sin \delta \cos \delta \frac{a'c'}{l^2} + \sin^2\delta \left(\frac{c'}{l}\right)^2 \right] \quad (21g)$$

$$C_{n_{\beta_2}} = C_{n_{\beta_1}} - 2K \cos \eta \sin \Gamma \cos \delta \left(\sin \Gamma \cos \delta \frac{a'}{l} + \sin \delta \frac{b'}{l} \right) \quad (21h)$$

$$C_{l_{\beta_2}} = C_{l_{\beta_1}} + 2K \cos \eta \sin \Gamma \cos \delta \left(\cos \Gamma \cos \delta \frac{b'}{l} + \sin \Gamma \cos \delta \frac{c'}{l} \right) \quad (21i)$$

$$C_{l_{p_2}} = C_{l_{p_1}} - 2K \cos \eta \cos^2\delta \left[\cos^2\Gamma \left(\frac{b'}{l}\right)^2 + 2 \sin \Gamma \cos \Gamma \frac{b'c'}{l^2} + \sin^2\Gamma \left(\frac{c'}{l}\right)^2 \right] \quad (21j)$$

$$C_{l_{r_2}} = C_{l_{r_1}} + 2K \cos \eta \cos \delta \left[\sin \Gamma \left(\cos \Gamma \cos \delta \frac{a'b'}{l^2} + \sin \delta \frac{b'c'}{l^2} + \sin \Gamma \cos \delta \frac{a'c'}{l^2} \right) + \cos \Gamma \sin \delta \left(\frac{b'}{l}\right)^2 \right] \quad (21k)$$

$$C_{n_{p_2}} = C_{n_{p_1}} + 2K \cos \eta \cos \delta \left[\sin \Gamma \left(\cos \Gamma \cos \delta \frac{a'b'}{l^2} + \sin \delta \frac{b'c'}{l^2} + \sin \Gamma \cos \delta \frac{a'c'}{l^2} \right) + \cos \Gamma \sin \delta \left(\frac{b'}{l}\right)^2 \right] \quad (21l)$$

$$C_{n_{r_2}} = C_{n_{r_1}} - 2K \cos \eta \left[\sin^2\Gamma \cos^2\delta \left(\frac{a'}{l}\right)^2 + 2 \sin \Gamma \sin \delta \cos \delta \frac{a'b'}{l^2} + \sin^2\delta \left(\frac{b'}{l}\right)^2 \right] \quad (21m)$$

where a', b', and c' are the distances in the x-, y-, and z-directions, respectively, from the first moment reference center to the second moment reference center.

SELECTION OF K

According to Newtonian theory, the value of K should be 2. However, it is shown in references 1, 7, 8, and 10 that more accurate predictions of experimental results can be obtained if the value of K is chosen to give the correct value for the stagnation pressure coefficient.

For blunt bodies the value of the stagnation pressure coefficient is

$$C_{p,s} = 2 - \frac{\rho_\infty}{\rho} = \frac{\gamma + 3}{\gamma + 1}\left(1 - \frac{2}{\gamma + 3}\frac{1}{M_\infty^2}\right) \tag{22}$$

Thus, at large angles of attack (near 90°), the constant K should have the value of equation (22). This value of K should also be used in the relations for the hemicylindrical leading edge (appendix A) and the spherical wedge nose (appendix B).

For a flat surface with an attached shock the constant-density solution (ref. 7), which in the case of the flat surface is the "exact" solution, gives for the pressure coefficient on the surface

$$C_p = \frac{2\sin^2\alpha}{\left(1 - \frac{\rho_\infty}{\rho}\right)\cos^2(\sigma - \alpha)} = 2\left(1 - \frac{\rho_\infty}{\rho}\right)\sin^2\sigma \tag{23}$$

where the density ratio is

$$\frac{\rho_\infty}{\rho} = \left(\frac{\gamma - 1}{\gamma + 1}\right)\left(1 + \frac{2}{\gamma - 1}\frac{1}{M_\infty^2\sin^2\sigma}\right) \tag{24}$$

If $\left(\frac{\rho_\infty}{\rho}\right)^{1/2} \tan\alpha$ is small, the factor $\cos^{-2}(\sigma - \alpha)$ may be omitted; and if $M_\infty^2\sin^2\sigma \gg 1$, the value for the pressure coefficient may be approximated by

$$C_p = (\gamma + 1)\sin^2\alpha \tag{25}$$

This result is similar to that obtained from the small-disturbance theory of reference 11 when the assumption $M_\infty^2 \sin^2\alpha \gg 1$ is used. The Newtonian value for the pressure coefficient on an inclined flat plate is simply

$$C_p = 2 \sin^2\alpha$$

Thus, at low angles of attack up to the detachment angle the constant K should have the value $\gamma + 1$.

The second form of equation (23), which is an "exact" relation, suggests that the modified Newtonian theory could be applied to the attached shock case, even when $M_\infty^2 \sin^2\sigma$ is not very much greater than unity, provided that the shock angle σ is used in the Newtonian relations rather than the surface angle α.

The proper value of γ to be used in determining K is a function of both the Mach number normal to the oblique shock, $M_\infty \sin\sigma$, and the altitude. A discussion of the variation of an effective value of γ which includes the effects of ionization and dissociation for air is given in reference 12, and a plot of this variation from this reference is presented in figure 6. This figure was obtained by use of the 1956 model atmosphere of reference 13. (Note that figure 6 contains data from references 14 and 15.) Use of a more recent model atmosphere would change these curves somewhat. Results incorporating the latest altitude revisions may be obtained as indicated in reference 12.

APPLICATION OF METHOD

Before a specific example to illustrate use of the method is attempted, the assumptions and restrictions which have been incorporated in equations (17) are recapitulated for convenient reference:

(1) Equations (17) are restricted to only those surfaces which "see" the flow, a condition which may be expressed by $\cos\eta \leqq 0$. When the surface does not see the flow it is assumed that $C_p = 0$.

(2) Equations (17) are restricted to zero sideslip angle ($\beta = 0$).

(3) Equations (17) are strictly valid only for small oscillations about the equilibrium, or trim, condition, because the small-angle approximation was used. This approximation permitted retention of only first-order terms in the expressions for the static stability derivatives.

(4) The rotational velocity parameters $\frac{pl}{V_\infty}$, $\frac{ql}{V_\infty}$, and $\frac{rl}{V_\infty}$ are assumed to be vanishingly small in comparison with unity. This condition appears to be realistic in view of the extreme flight velocities to which the method applies.

In order to illustrate the procedure used in evaluating the aerodynamic coefficients, consider the configuration shown in figure 7. This configuration consists of flat-plate wing panels, elevons, and vertical surfaces with hemicylindrical leading edges. Configuration dimensions (in terms of the length l) and surface angles are given in figure 7. The center of gravity of the configuration is located $0.594l$ behind the apex of the wing surface.

For purposes of calculation the configuration is considered to consist of six separate flat surfaces. These surfaces are the right- and left-hand wing panels, the right- and left-hand elevons, and the right- and left-hand vertical surfaces. The geometric properties of these components are presented in table I. Also, the double integral expressions of equations (17) were computed by means of equations (20) and listed in this table. Next the values of the normal-force, axial-force, and pitching-moment coefficients were calculated by use of equations (17), figure 4, and the results of table I for the individual surfaces for an angle-of-attack range of 20° to 60°. For this angle-of-attack range the fuselage was completely hidden from the flow. These coefficients were then based on the total configuration planform area by multiplying by the ratio S_i/S_{tot}, where S_i indicates the area of the component surface. Finally, coefficients for all components were summed to determine the values for the complete configuration. These values of normal-force, axial-force, and pitching-moment coefficients are presented as functions of angle of attack in figure 8. The Newtonian value of 2 was used for the constant K throughout these calculations.

The effects of leading-edge bluntness were also calculated by the method of appendix A. Six separate edges were considered: the right- and left-hand leading edges of the wing panel, the right- and left-hand edges at the tip of the wing (these edges fair into the vertical surfaces so that the value for the angle ξ was zero for all angles of attack), and the leading edges of the right- and left-hand vertical surfaces. The pitching-moment contribution of the blunt edges was computed from the normal- and axial-force coefficients and the x- and z-components of the lengths from the center of gravity of the configuration to the midpoint of the longitudinal axes of the hemicylinders which formed the edges. The contribution of the spherical-wedge nose section to the normal- and axial-force coefficients was computed by the method of appendix B. For this computation the dihedral angle was assumed to be 0°. The effect of this approximation is negligible for this case where

the actual dihedral angle was only 10°. The pitching-moment contribution of the spherical-wedge nose section was calculated from the values of the normal- and axial-force coefficients and the distances in the x- and z-directions from the configuration center of gravity to the origin of the spherical-wedge section.

The normal-force, axial-force, and pitching-moment coefficients for the complete configuration including the effects of blunt nose and leading edges are shown as functions of angle of attack in figure 8. The various stability derivatives were then calculated for the configuration at the trim angle of attack of 40°. The results of these calculations, which represent the sum of the contributions of the six flat-plate surfaces (the effects of blunt leading edges were not included), are presented below:

L
1
6
9
1

$$C_{m_\alpha} = -0.0368$$

$$C_{l_\beta} = -0.0356$$

$$C_{n_\beta} = -0.0005$$

$$C_{Y_\beta} = -0.0650$$

$$C_{m_q} = -0.1139$$

$$C_{l_p} = -0.0499$$

$$C_{l_r} = -0.0002$$

$$C_{n_p} = -0.0002$$

$$C_{n_r} = -0.0042$$

If the leading edge was so blunt that its contribution to the stability derivatives was important it could be approximated (for the purpose of obtaining stability derivatives) by several flat-plate sections.

CONCLUDING REMARKS

A method, based on the modified Newtonian theory, for calculating aerodynamic forces, moments, and stability derivatives at zero sideslip angle for combinations of flat plates of arbitrary planform shape and

orientation is presented. Methods for predicting the aerodynamic forces on hemicylindrical leading edges and spherical-wedge nose sections are also presented. Equations are derived and several design-type charts are presented to facilitate computation. The method is illustrated by a sample calculation. Values of the multiplicative factor used in modifying the Newtonian impact theory to account for variations in Mach number and the ratio of specific heats are discussed.

Langley Research Center,
National Aeronautics and Space Administration,
Langley Air Force Base, Va., November 8, 1961.

APPENDIX A

FORCE COEFFICIENTS FOR HEMICYLINDRICAL LEADING EDGES

A sketch of a hemicylindrical leading edge is shown in figure 9(a). To facilitate the analysis the leading edge will be considered to consist of a squared leading-edge section (figs. 9(b) and 9(c)) and the end sections (figs. 9(d) and 9(e)). The analysis for either end is similar and the results are equivalent so only one end section is considered in this appendix.

The squared leading-edge section.- The unit vector parallel to the leading edge can be written in terms of the body system of axes as

$$\vec{U} = \vec{i}\cos\delta\sin(\Lambda+\epsilon) + \vec{j}\left[\sin\delta\sin\Gamma\sin(\Lambda+\epsilon) - \cos\Gamma\cos(\Lambda+\epsilon)\right] + \vec{k}\left[-\sin\delta\cos\Gamma\sin(\Lambda+\epsilon) - \sin\Gamma\cos(\Lambda+\epsilon)\right] = \vec{i}U_x + \vec{j}U_y + \vec{k}U_z \tag{A1}$$

The effective sweep angle is defined by the expression

$$\vec{V}_\infty\cdot\vec{U} = -V_\infty\sin\Lambda_e \tag{A2}$$

combining equations (3), (A1), and (A2), yields

$$\sin\Lambda_e = U_x\cos\alpha\cos\beta + U_y\sin\beta + U_z\sin\alpha\cos\beta \tag{A3}$$

From figure 9(c), which shows the hemicylindrical leading edge cut by a plane normal to the unit vector $\vec{U}$, the pressure coefficient may be written

$$C_p = K\left(\frac{V_{N,s}}{V_\infty}\right)^2\cos^2\theta \tag{A4}$$

where θ is the angle between the normal-velocity component at the stagnation point and the point at which the pressure coefficient is to be computed.

The normal-velocity component at the stagnation point is given by

$$\vec{V}_{N,s} = \vec{V}_\infty - \left(\vec{V}_\infty\cdot\vec{U}\right)\vec{U} = \vec{V}_\infty + \vec{U}V_\infty\sin\Lambda_e \tag{A5}$$

and

$$V_{N,s} = V_\infty \cos \Lambda_e$$

so that

$$C_p = K \cos^2\Lambda_e \cos^2\theta \tag{A6}$$

The angle ξ defined in figure 8(c) is given by the expression

$$\vec{V}_{N,s}\cdot\vec{n} = -V_{N,s} \cos \xi$$

or

$$\cos \xi = \frac{1}{\cos \Lambda_e}(\cos \alpha \cos \beta \sin \delta - \sin \beta \sin \Gamma \cos \delta + \sin \alpha \cos \beta \cos \Gamma \cos \delta) \tag{A7}$$

The normal-force contribution of the squared leading-edge section is given by

$$C_N = \frac{1}{2RL} \int_{-\xi}^{\pi/2} \int_0^L C_p \vec{k}\cdot\vec{r} R \, d\theta \, dU \tag{A8}$$

where

$$\vec{r} = \left(- \frac{\vec{V}_{N,s}}{V_{N,s}} \cos \theta + \frac{\vec{U} \times \vec{V}_\infty}{\left|\vec{U} \times \vec{V}_\infty\right|} \sin \theta \right)$$

is the unit radius vector.

The scalar product $\vec{k}\cdot\vec{r}$ becomes, after suitable algebraic manipulation,

$$\vec{k}\cdot\vec{r} = \frac{1}{\cos \Lambda_e}(N_1 \cos \theta + N_2 \sin \theta)$$

where

$$N_1 = -(U_z \sin \Lambda_e - \sin \alpha \cos \beta)$$

$$N_2 = -(U_x \sin \beta - U_y \cos \alpha \cos \beta)$$

Upon substitution of these expressions into equation (A8) and performance of the required integrations the normal-force coefficient for the squared leading-edge section becomes

$$C_N = \frac{K}{2} \cos \Lambda_e \left[N_1 f_1(\xi) + N_2 f_2(\xi) \right] \tag{A9}$$

where

$$f_1(\xi) = \frac{1}{3}\left[2 + \sin \xi (2 + \cos^2 \xi) \right]$$

$$f_2(\xi) = \frac{1}{3} \cos^3 \xi$$

Curves of these functions are presented in figure 10. When values for $\cos \Lambda_e$ and $\cos \xi$ from $\sin \Lambda_e$ and $\sin \xi$, respectively, are computed, care must be taken in determining the quadrant of the angle so that the cosine values will have the proper signs.

The axial-force and side-force coefficients for the squared leading-edge section can be determined in a manner similar to that which was used for the normal-force coefficients. The resulting expressions are

$$C_A = \frac{K}{2} \cos \Lambda_e \left[A_1 f_1(\xi) + A_2 f_2(\xi) \right] \tag{A10}$$

where

$$A_1 = -(U_x \sin \Lambda_e - \cos \alpha \cos \beta)$$

$$A_2 = -(U_y \sin \alpha \cos \beta - U_z \sin \beta)$$

and

$$C_Y = \frac{K}{2} \cos \Lambda_e \left[Y_1 f_1(\xi) + Y_2 f_2(\xi) \right] \tag{A11}$$

where

$$Y_1 = U_y \sin \Lambda_e - \sin \beta$$

$$Y_2 = -(U_x \sin \alpha \cos \beta - U_z \cos \alpha \cos \beta)$$

Expressions for the moment coefficients have not been presented, since these moments are always zero at a point which lies on the longitudinal axis of the hemicylinder and is midway between the ends of the hemicylinder. That the moments are zero at this point can be seen from the fact that the force on any increment of the surface is always directed toward the center of curvature of the surface, which, in the case of the hemicylinder, is located on the longitudinal axis.

Although the analysis is similar for both the squared leading-edge section (fig. 9(b)) and the end section (fig. 9(d)), these sections are treated separately because the limits of integration of the pressure coefficient over the surface are different.

When $\frac{\pi}{2} \geqq \lambda \geqq \xi$, the upper limit of integration with respect to θ is $\frac{\pi}{2}$, as was the case for the squared section, and the lower limit of integration becomes $\frac{\pi}{2} - (\xi + \lambda)$. The angle λ may be expressed as a function of U and τ as

$$\cos \lambda = \frac{U}{R} \cot \tau \tag{A12}$$

L
1
6
9
1

When $\frac{\pi}{2} \geqq \lambda \geqq \xi$, the value of U is restricted to $0 \leqq U \leqq R \tan \tau \cos \xi$ so that the upper and lower limits of integration with respect to U are $R \tan \tau \cos \xi$ and 0, respectively.

When $\xi \geqq \lambda \geqq 0$, the upper limit of integration with respect to θ is $\frac{\pi}{2} - (\xi - \lambda)$ and the lower limit remains $\frac{\pi}{2} - (\xi + \lambda)$. For this case the value of U is restricted to $R \tan \tau \cos \xi \leqq U \leqq R \tan \tau$, so that the upper and lower limits of integration with respect to U become $R \tan \tau$ and $R \tan \tau \cos \xi$, respectively.

The normal-force contribution of the end section of the leading edge is given by

$$C_N = -\frac{1}{2R^2 \tan} \left[\int_0^{R \tan \tau \cos \xi} \int_{\pi/2-(\xi+\lambda)}^{\pi/2} C_p \vec{k} \cdot \vec{r} R \, d\theta \, dU \right.$$

$$\left. + \int_{R \tan \tau \cos \xi}^{R \tan \tau} \int_{\pi/2-(\xi+\lambda)}^{\pi/2-(\xi-\lambda)} C_p \vec{k} \cdot \vec{r} R \, d\theta \, dU \right] \tag{A13}$$

Upon integration the normal-force coefficient becomes

$$C_N = \frac{K}{2} \cos \Lambda_e \left[N_1 f_3(\xi) + N_2 f_4(\xi) \right] \tag{A14}$$

where

$$f_3(\xi) = \frac{3}{8}\left[\cos\ \xi\left(1 - \frac{1}{3}\cos^2\xi\right) + \left(\frac{\pi}{2} + \xi\right)\sin\ \xi\right]$$

$$f_4(\xi) = \frac{1}{8}\left[\sin\ \xi\ \cos^2\xi + \left(\frac{\pi}{2} + \xi\right)\cos\ \xi\right]$$

Curves of the functions $f_3(\xi)$ and $f_4(\xi)$ are presented in figure 10.

The axial-force and side-force coefficients for the end section of the leading edge are obtained in a similar manner with the results

$$C_A = \frac{K}{2}\cos\ \Lambda_e\left[A_1 f_3(\xi) + A_2 f_4(\xi)\right] \tag{A15}$$

and

$$C_Y = \frac{K}{2}\cos\ \Lambda_e\left[Y_1 f_3(\xi) + Y_2 f_4(\xi)\right] \tag{A16}$$

It may be noted that an expression for the effective sweep angle may be found in terms of the parameters N_2, A_2, Y_2. The expression is

$$\cos\ \Lambda_e = \sqrt{N_2^2 + A_2^2 + Y_2^2}$$

Similarly, an expression for the angle ξ may be found in terms of the parameters N_1, A_1, and Y_1. This expression is

$$\cos\ \xi = \frac{N_1 \cos\ \Gamma \cos\ \delta + A_1 \sin\ \delta + Y_1 \sin\ \Gamma \cos\ \delta}{\cos\ \Lambda_e} \tag{A17}$$

APPENDIX B

FORCE COEFFICIENTS FOR A SPHERICAL-WEDGE NOSE SECTION

The apex of a swept wing with hemicylindrical leading edges is often rounded by making the nose a spherical-wedge section provided the surface orientation angles Γ and ϵ of the wing panels are zero. If these angles are not zero, the nose is not a spherical-wedge section but would be approximated by one if both Γ and ϵ are small.

The pressure coefficient for impact theory on a spherical-wedge nose section is given by the expression

$$C_p = K\left(\frac{\vec{V}_\infty \cdot \vec{r}}{V_\infty}\right)^2 \tag{B1}$$

where the unit radial vector $\vec{r}$ is given by (fig. 11):

$$\vec{r} = \vec{i}(\cos\delta\cos\phi\cos\psi - \sin\delta\sin\psi) - \vec{j}\sin\phi\cos\psi - \vec{k}(\sin\delta\cos\phi\cos\psi + \cos\delta\sin\psi) \tag{B2}$$

Thus, the pressure coefficient is

$$C_p = K\left[\sin(\alpha+\delta)\cos\beta\sin\psi - \cos(\alpha+\delta)\cos\beta\cos\phi\cos\psi + \sin\beta\sin\phi\cos\psi\right]^2 \tag{B3}$$

The normal-force coefficient is given by

$$C_N = \frac{K}{\pi R^2}\int_{-\pi/2}^{\psi_o}\int_0^{\phi_o} C_p\,\vec{k}\cdot\vec{r}R^2\cos\psi\,d\phi\,d\psi \tag{B4}$$

which becomes for the simple case when $\beta = 0^\circ$

$$C_N = \frac{2K}{\pi}\left[\cos\delta \int_{-\pi/2}^{\psi_o} \frac{\partial}{\partial\psi}\Phi(\alpha+\delta,\psi,\Lambda)d\psi - \sin\delta \int_{-\pi/2}^{\psi_o} \frac{\partial}{\partial\psi}\Psi(\alpha+\delta,\psi,\Lambda)d\psi\right] \quad (B5)$$

where, for $\tan(\alpha + \delta)\tan\psi > \cos\Lambda$,

$$\cos\phi_o = \tan(\alpha + \delta)\tan\psi \quad (B6a)$$

and, for $\tan(\alpha + \delta)\tan\psi \leqq \cos\Lambda$,

$$\cos\phi_o = \cos\Lambda \quad (B6b)$$

Also,

$$\frac{\partial}{\partial\psi}\Phi = -\sin\psi\cos\psi\left\{\left[\sin^2(\alpha + \delta)\sin^2\psi + \frac{1}{2}\cos^2(\alpha + \delta)\cos^2\psi\right]\cos^{-1}\left[\tan(\alpha + \delta)\tan\psi\right] + \sin(\alpha + \delta)\cos(\alpha + \delta)\left[2 + \frac{1}{2}\sin\psi\cos\psi\right]\sqrt{1 - \tan^2(\alpha + \delta)\tan^2\psi}\right\} \quad (B7)$$

$$\frac{\partial}{\partial\psi}\Psi = \cos^2\psi\left\{\frac{1}{3}\left[\sin^2(\alpha + \delta)\sin^2\psi + 2\cos^2(\alpha + \delta)\cos^2\psi\right]\sqrt{1 - \tan^2(\alpha + \delta)\tan^2\psi} - \sin(\alpha + \delta)\cos(\alpha + \delta)\sin\psi\cos\psi\cos^{-1}\left[\tan(\alpha + \delta)\tan\psi\right]\right\} \quad (B8)$$

and

$$\psi_o = \frac{\pi}{2} - (\alpha + \delta) \quad (B9)$$

Similarly,

$$C_A = \frac{2K}{\pi}\left[\sin\delta \int_{-\pi/2}^{\psi_o} \frac{\partial}{\partial\psi}\Phi(\alpha+\delta,\psi,\Lambda)d\psi + \cos\delta \int_{-\pi/2}^{\psi_o} \frac{\partial}{\partial\psi}\Psi(\alpha+\delta,\psi,\Lambda)d\psi\right] \quad (B10)$$

Values of Φ and Ψ for a range of values of $\alpha + \delta$ and Λ have been determined from graphical integration of equations (B7) and (B8), and the results are presented in figure 12. The normal-force and

axial-force coefficients due to the spherical-wedge nose section when $\beta = \Gamma = \epsilon = 0^{o}$ can be calculated from the expressions

$$\left.\begin{aligned} C_N &= \frac{2K}{\pi}(\Phi \cos \delta - \Psi \sin \delta) \\ C_A &= \frac{2K}{\pi}(\Phi \sin \delta + \Psi \cos \delta \end{aligned}\right\} \qquad \text{(B11)}$$

Expressions for the moment coefficients are not needed, inasmuch as the force on any increment of the surface is always directed toward the center of curvature of the surface and the moments are, therefore, always zero about the origin of a spherical surface.

REFERENCES

1. Lees, Lester: Hypersonic Flow. Fifth International Aeronautical Conference (Los Angeles, Calif., June 20-23, 1955), Inst. Aero. Sci., Inc., 1955, pp. 241-276.

2. Grimminger, G., Williams, E. P., and Young, G. B. W.: Lift on Inclined Bodies of Revolution in Hypersonic Flow. Jour. Aero. Sci., vol. 17, no. 11, Nov. 1950, pp. 675-690.

3. Rainey, Robert W.: Working Charts for Rapid Prediction of Force and Pressure Coefficients on Arbitrary Bodies of Revolution by Use of Newtonian Concepts. NASA TN D-176, 1959.

4. Tobak, Murray, and Wehrend, William R.: Stability Derivatives on Cones at Supersonic Speeds. NACA TN 3788, 1956.

5. Fisher, Lewis R.: Equations and Charts for Determining the Hypersonic Stability Derivatives of Combinations of Cone Frustums Computed by Newtonian Impact Theory. NASA TN D-149, 1959.

6. Margolis, Kenneth: Theoretical Evaluation of the Pressures, Forces, and Moments at Hypersonic Speeds Acting on Arbitrary Bodies of Revolution Undergoing Separate and Combined Angle-of-Attack and Pitching Motions. NASA TN D-652, 1961.

7. Hayes, Wallace D., and Probstein, Ronald F.: Hypersonic Flow Theory. Academic Press, Inc. (New York), 1959.

8. Penland, Jim A.: Aerodynamic Characteristics of a Circular Cylinder at Mach Number 6.86 and Angles of Attack up to 90°. NACA TN 3861, 1957. (Supersedes NACA RM L54A14.)

9. Anglin, Ernie L., and Scher, Stanley H.: Aerodynamic Requirements for Longitudinal Stability of Winged Space Vehicles Descending Into the Earth's Atmosphere at Very High Angles of Attack. Proc. Recovery of Space Vehicles Symposium (Los Angeles, Calif.), Inst. Aero. Sci., Aug. 31 - Sept. 1, 1960, pp. 32-34.

10. Love, Eugene S., Henderson, Arthur, Jr., and Bertram, Mitchel H.: Some Aspects of Air-Helium Simulation and Hypersonic Approximations. NASA TN D-49, 1959.

11. Van Dyke, Milton D.: A Study of Hypersonic Small Disturbance Theory. NACA Rep. 1194, 1954. (Supersedes NACA TN 3173.)

12. Trimpi, Robert L., and Jones, Robert A.: A Method of Solution With Tabulated Results for the Attached Oblique Shock-Wave System for Surfaces at Various Angles of Attack, Sweep, and Dihedral in an Equilibrium Real Gas Including the Atmosphere. NASA TR R-63, 1960.

13. Minzner, R. A., and Ripley, W. S.: The ARDC Model Atmosphere, 1956. Air Force Surveys in Geophysics No. 86 (AFCRC TN-56-204, ASTIA Doc. 110233), Air Force Cambridge Res. Center, Dec. 1956.

14. Huber, Paul W.: Tables and Graphs of Normal-Shock Parameters at Hypersonic Mach Numbers and Selected Altitudes. NACA TN 4352, 1958.

15. Feldman, Saul: Hypersonic Gas Dynamic Charts for Equilibrium Air. AVCO Res. Lab., Jan. 1957.

TABLE I.- GEOMETRIC PROPERTIES OF FLAT SURFACES OF CONFIGURATION SHOWN IN FIGURE 7

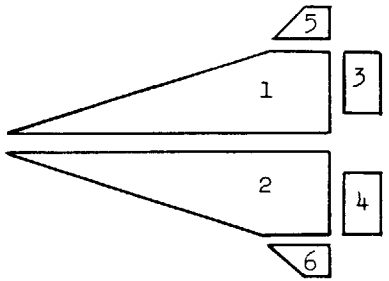

Component	S_i/l^2	a_i/l	b_i/l	c_i/l	$\bar{I}_{X,i}/l^4$	$\bar{I}_{Y,i}/l^4$	$\bar{I}_{XY,i}/l^4$
1	0.140	0.006	0.099	0.033	0.00066	0.00750	0.00090
2	.140	.006	-.099	.033	.00066	.00750	-.00090
3	.020	-.353	.150	.007	.00007	.00002	0
4	.020	-.353	-.150	.007	.00007	.00002	0
5	.015	-.228	.254	-.048	.00001	.00003	.00001
6	.015	-.228	-.254	-.048	.00001	.00003	-.00001

Component	$\iint_S \left(\frac{x}{l}\right)\frac{dS}{S}$	$\iint_S \left(\frac{y}{l}\right)\frac{dS}{S}$	$\iint_S \left(\frac{z}{l}\right)\frac{dS}{S}$	$\iint_S \left(\frac{x}{l}\right)^2\frac{dS}{S}$	$\iint_S \left(\frac{y}{l}\right)^2\frac{dS}{S}$	$\iint_S \left(\frac{z}{l}\right)^2\frac{dS}{S}$	$\iint_S \left(\frac{xy}{l^2}\right)\frac{dS}{S}$	$\iint_S \left(\frac{yz}{l^2}\right)\frac{dS}{S}$	$\iint_S \left(\frac{zx}{l^2}\right)\frac{dS}{S}$
1	0.0120	0.0990	0.0330	0.0537	0.0143	0.0012	0.0075	0.0024	-0.0007
2	.0120	-.0990	.0330	.0537	.0143	.0012	-.0075	-.0024	-.0007
3	-.3470	.1500	.0070	.1212	.0258	.0002	-.0520	.0005	-.0021
4	-.3470	-.1500	.0070	.1212	.0258	.0002	.0520	-.0005	-.0021
5	-.2220	.2540	-.0480	.0515	.0645	.0031	-.0564	-.0123	0100
6	-.2220	-.2540	-.0480	.0515	.0645	.0031	.0564	.0123	.0100

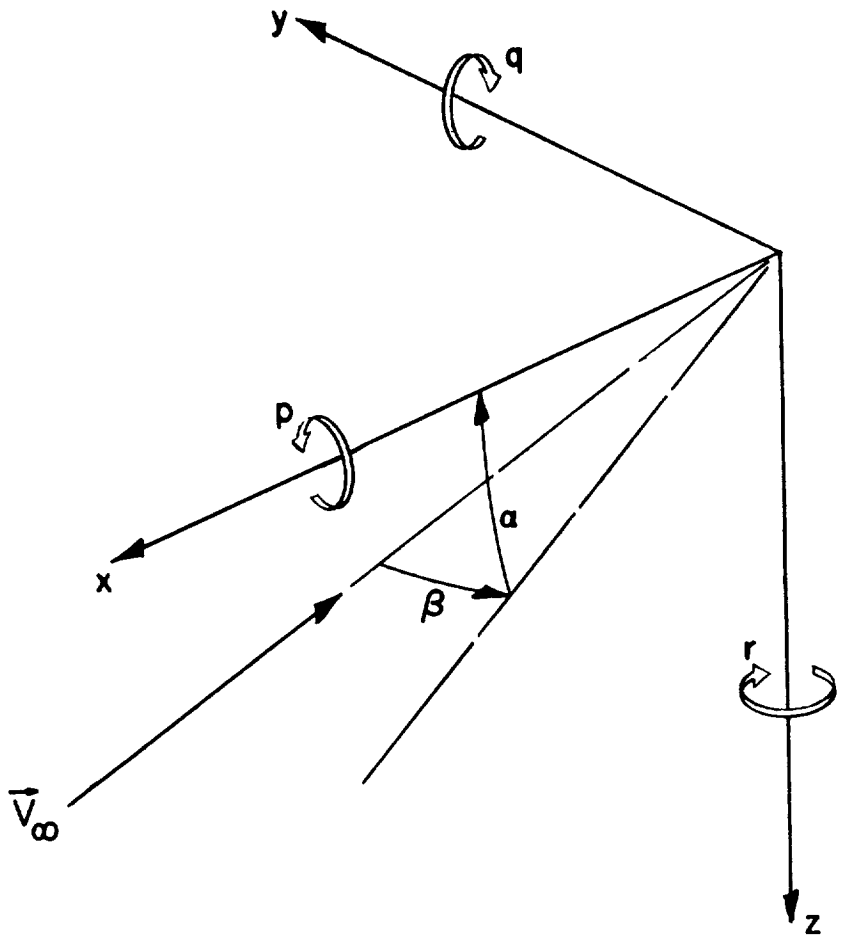

Figure 1.- Sketch showing positive directions of body system of axes, flow-direction angles, and rotational velocities.

I-1691

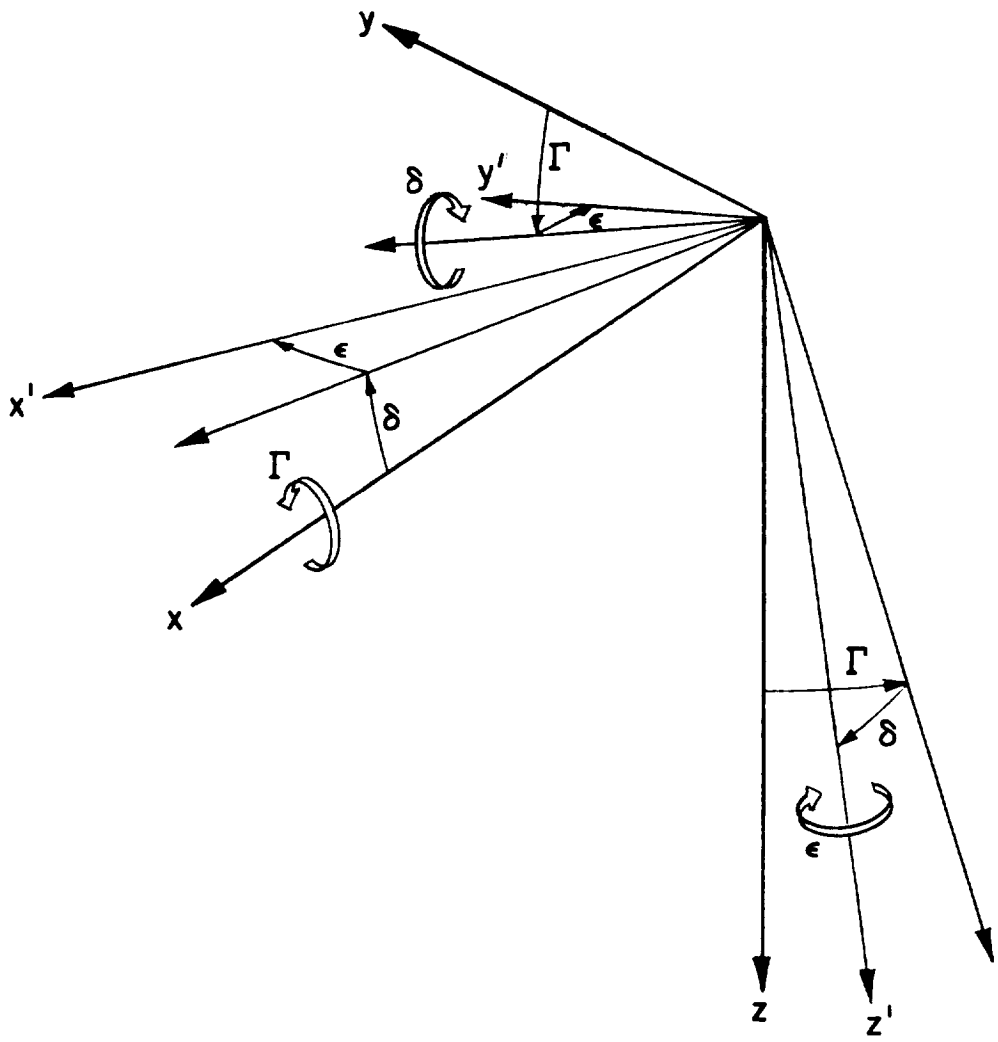

Figure 2.- Sketch showing positive directions of surface orientation angles. Undeflected surface lies in XY-plane of body-axis system.

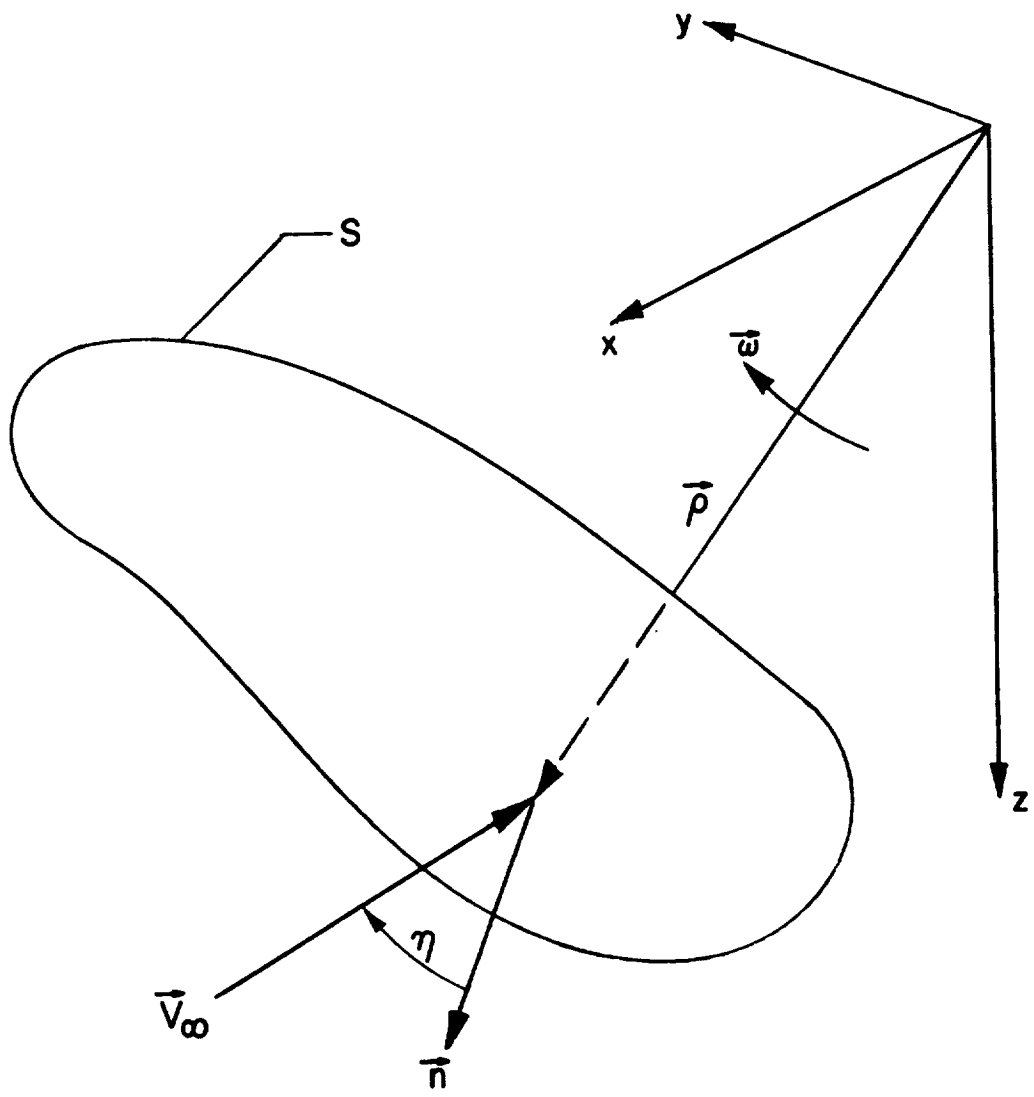

Figure 3.- Arbitrary flat surface rotating about the origin of the body system of axes with angular velocity $\vec{\omega}$.

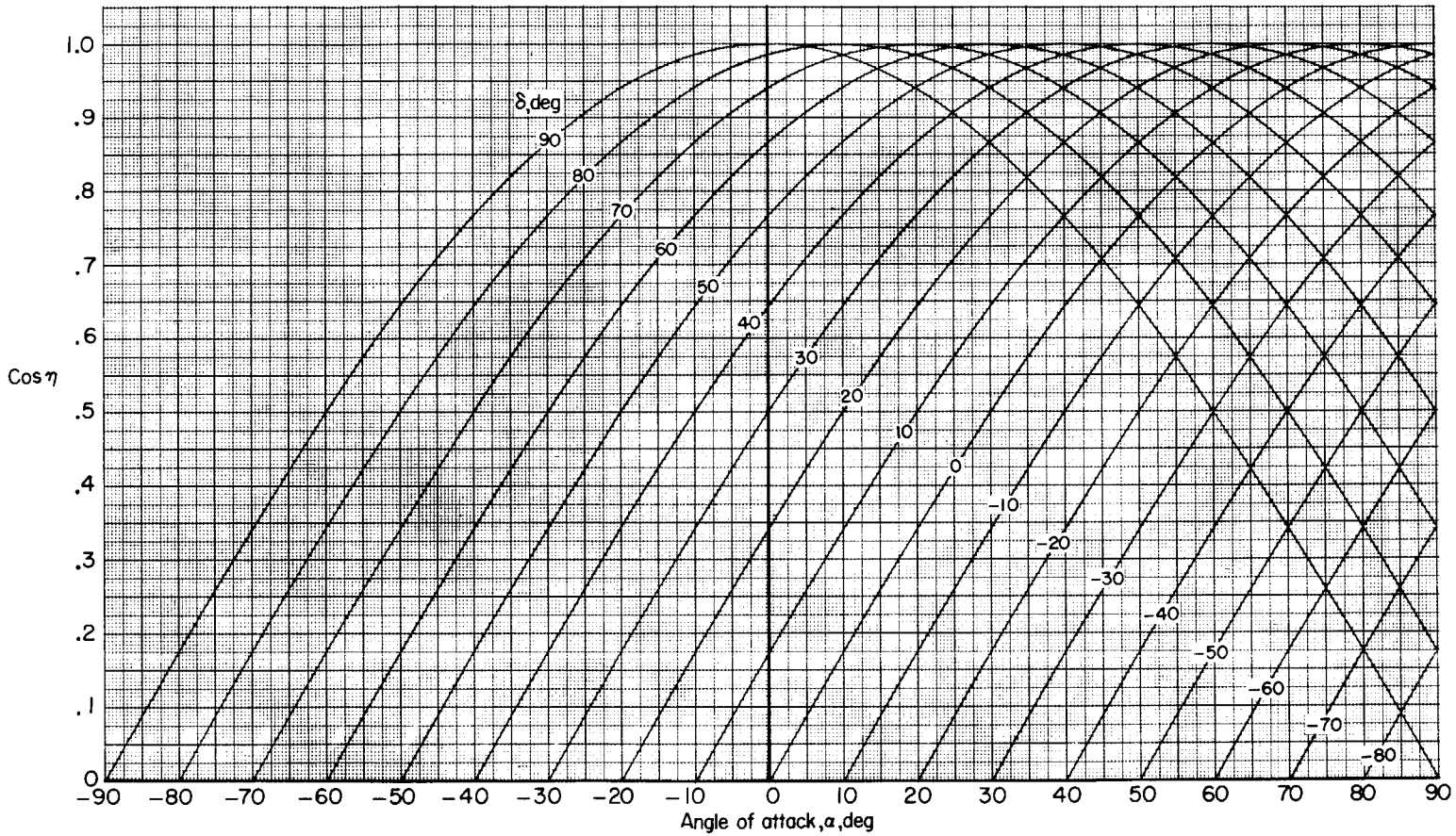

(a) $\Gamma = 0^{\circ}$.

Figure 4.- Variation of the parameter $\cos \eta$ with angle of attack for various values of the surface orientation angles Γ and δ. $\beta = 0^{\circ}$.

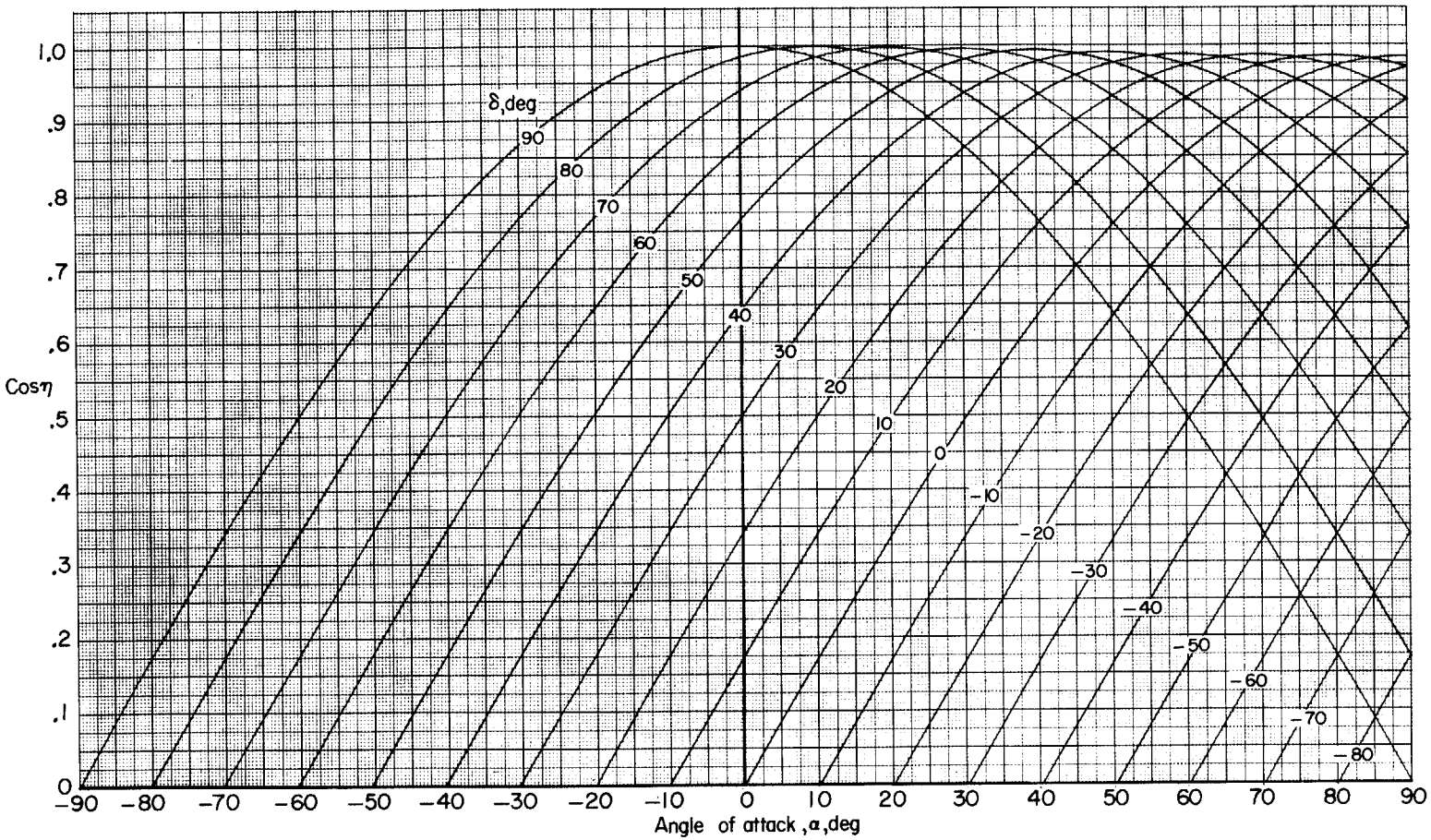

(b) $\Gamma = \pm 10^{o}$.

Figure 4.- Continued.

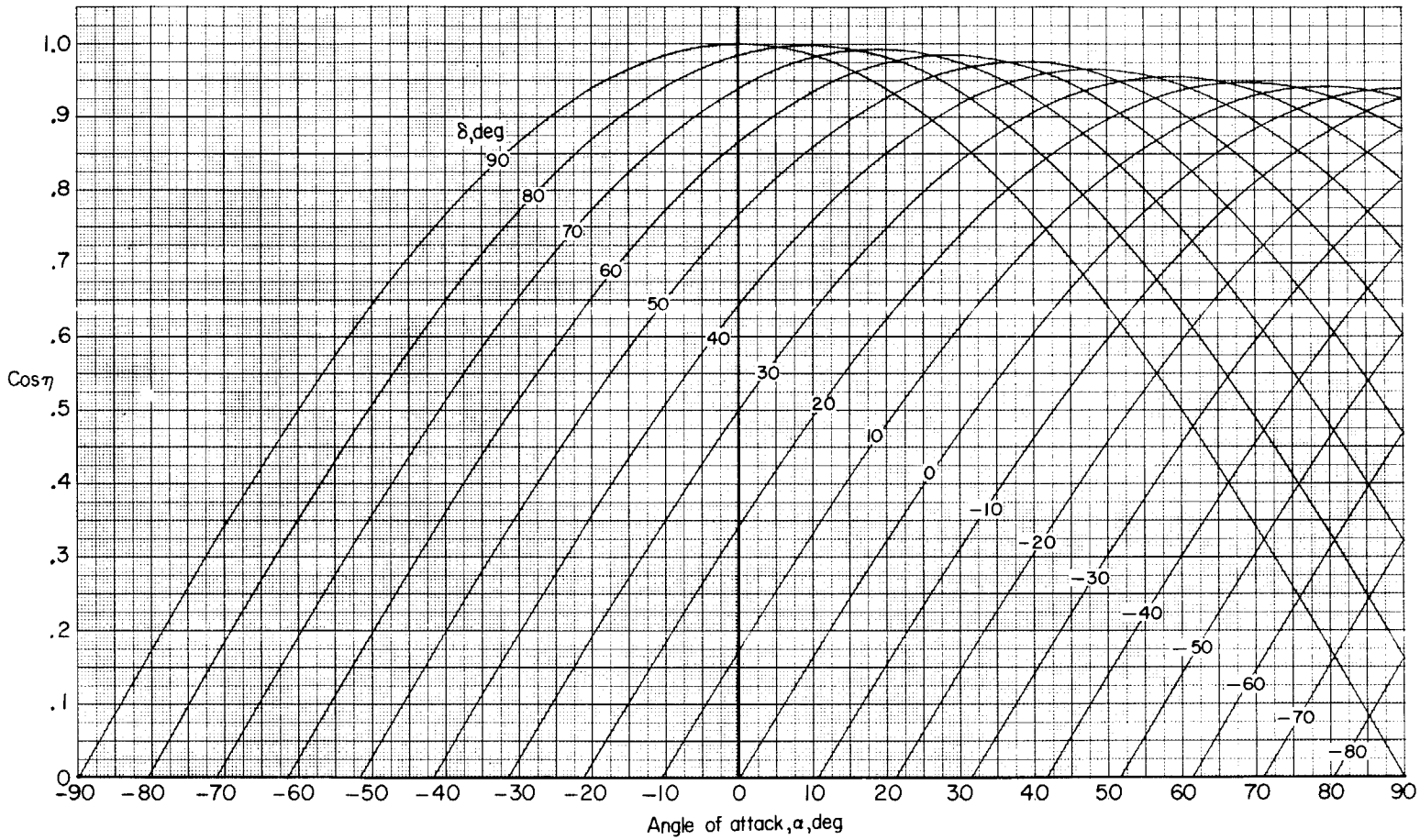

(c) $\Gamma = \pm 20^{\circ}$.

Figure 4.- Continued.

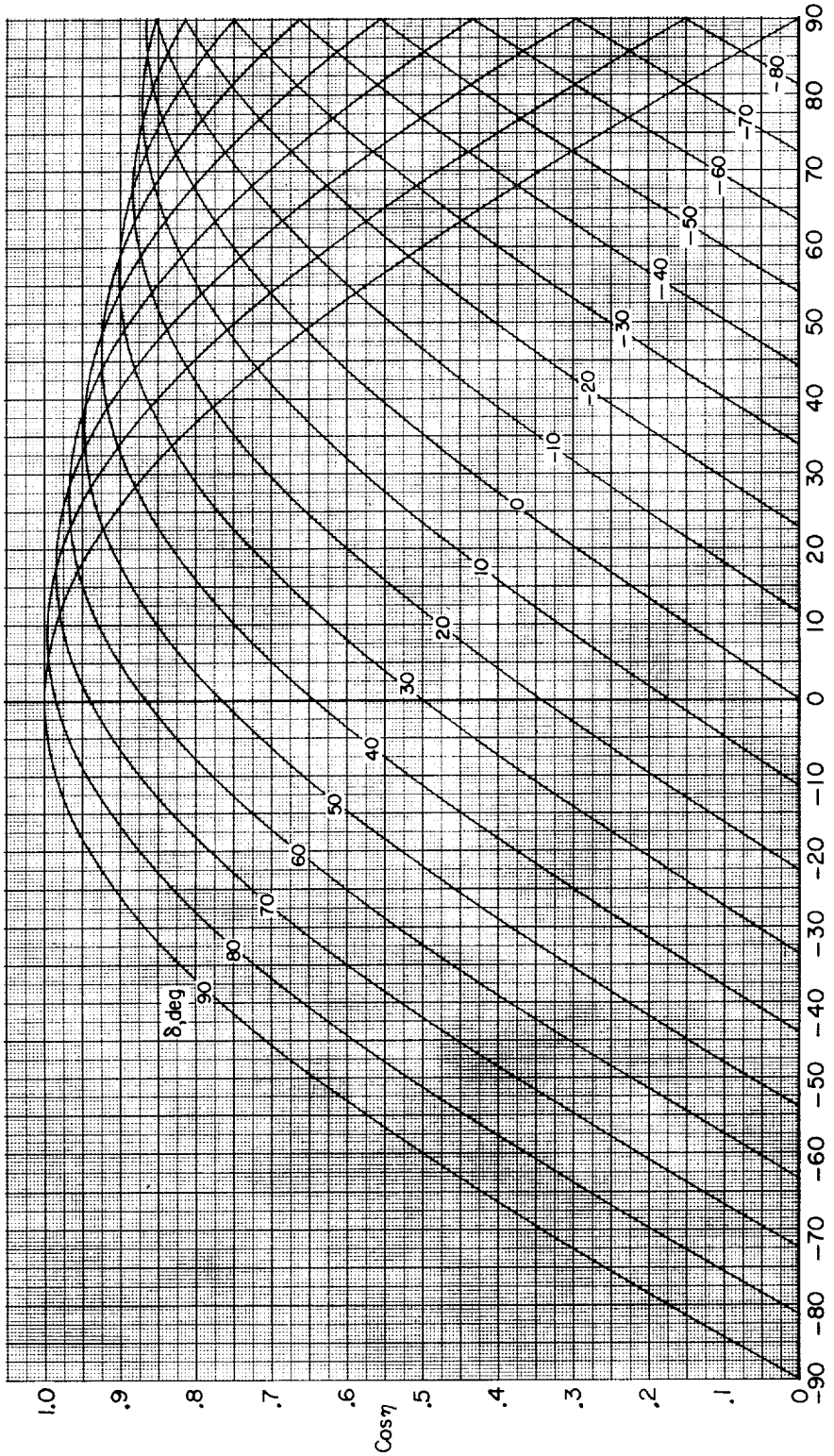

(d) $\Gamma = \pm 30^{\circ}$.

Figure 4.- Continued.

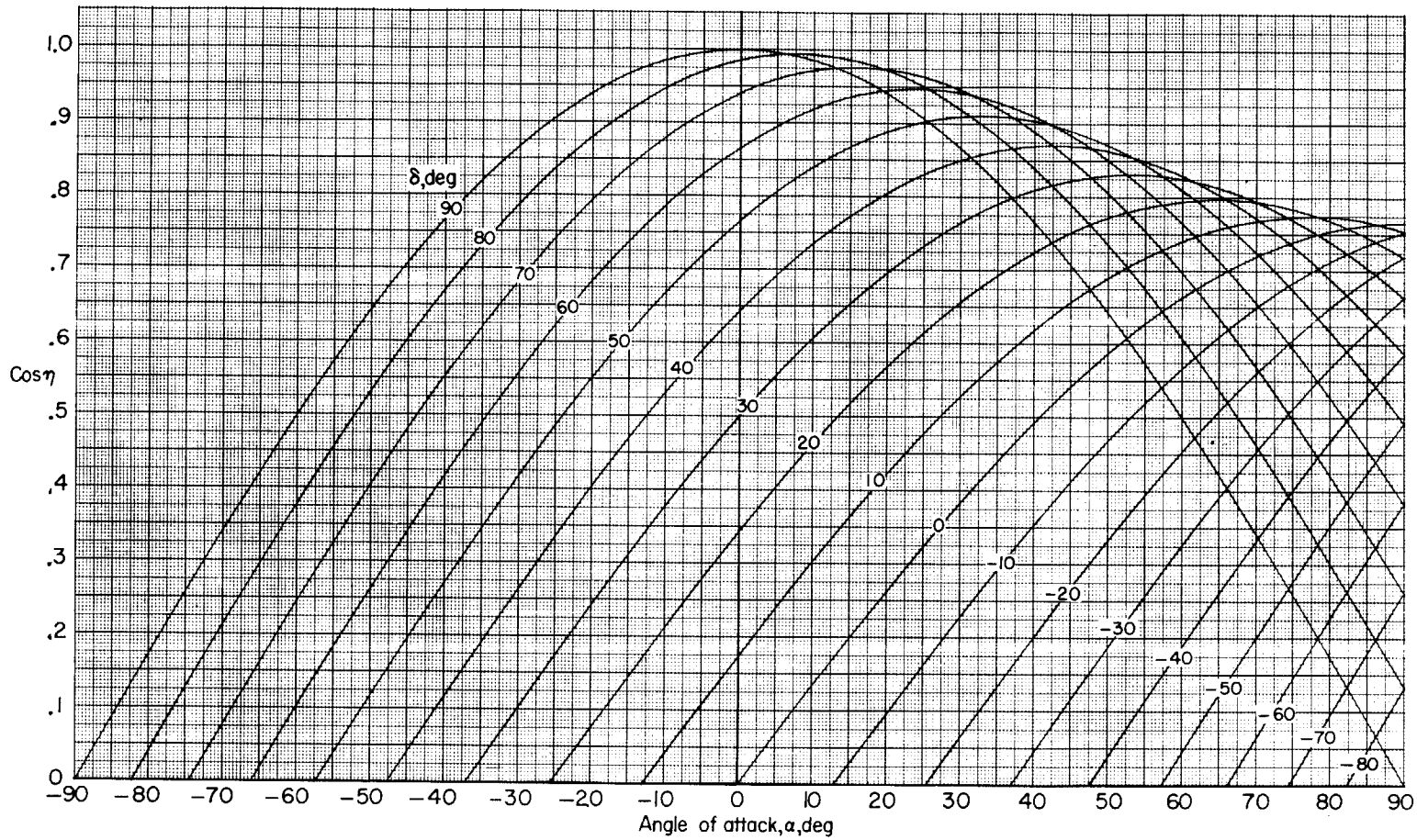

(e) $\Gamma = \pm 40^{\circ}$.

Figure 4.- Continued.

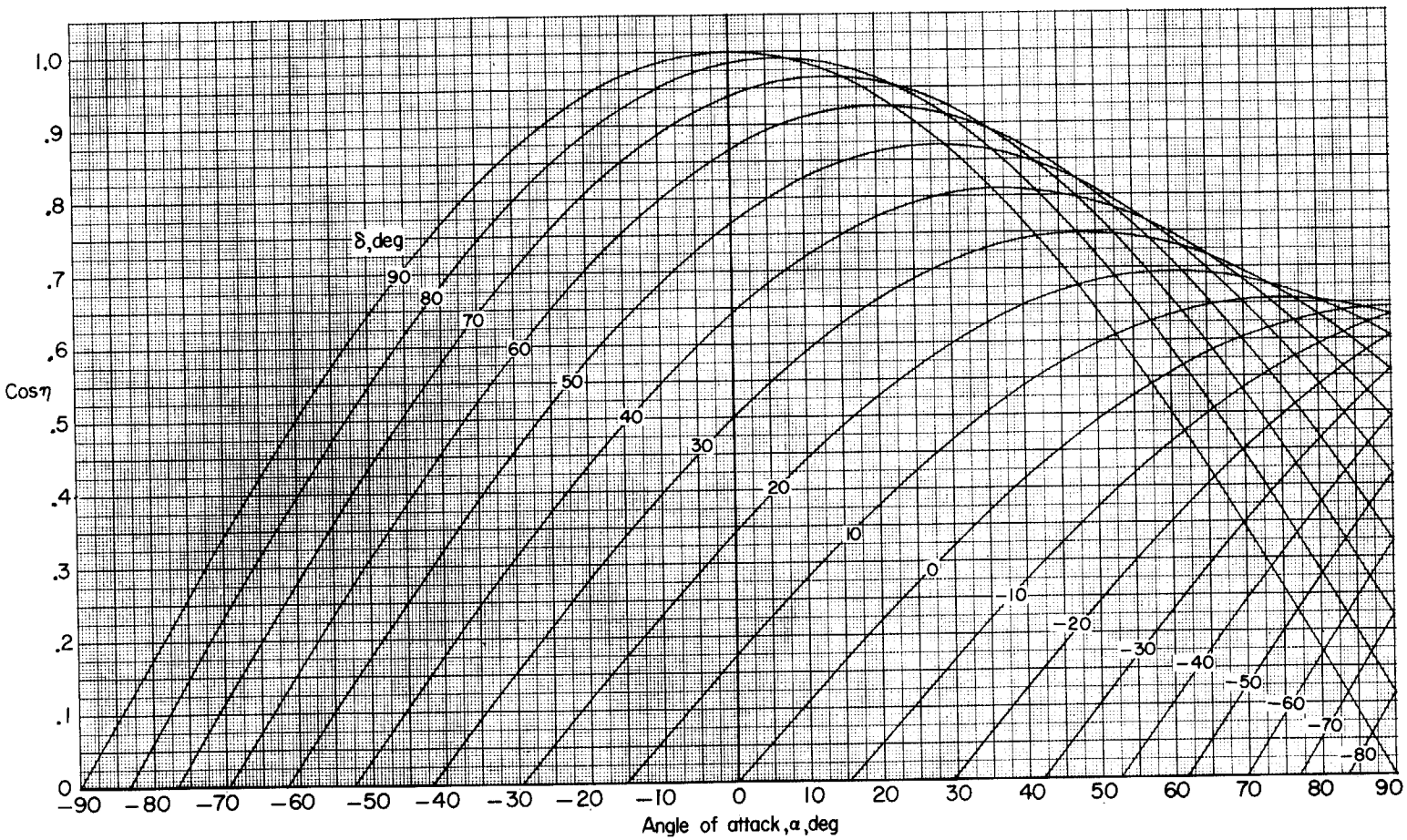

(f) $\Gamma = \pm 50^{\circ}$.

Figure 4.- Continued.

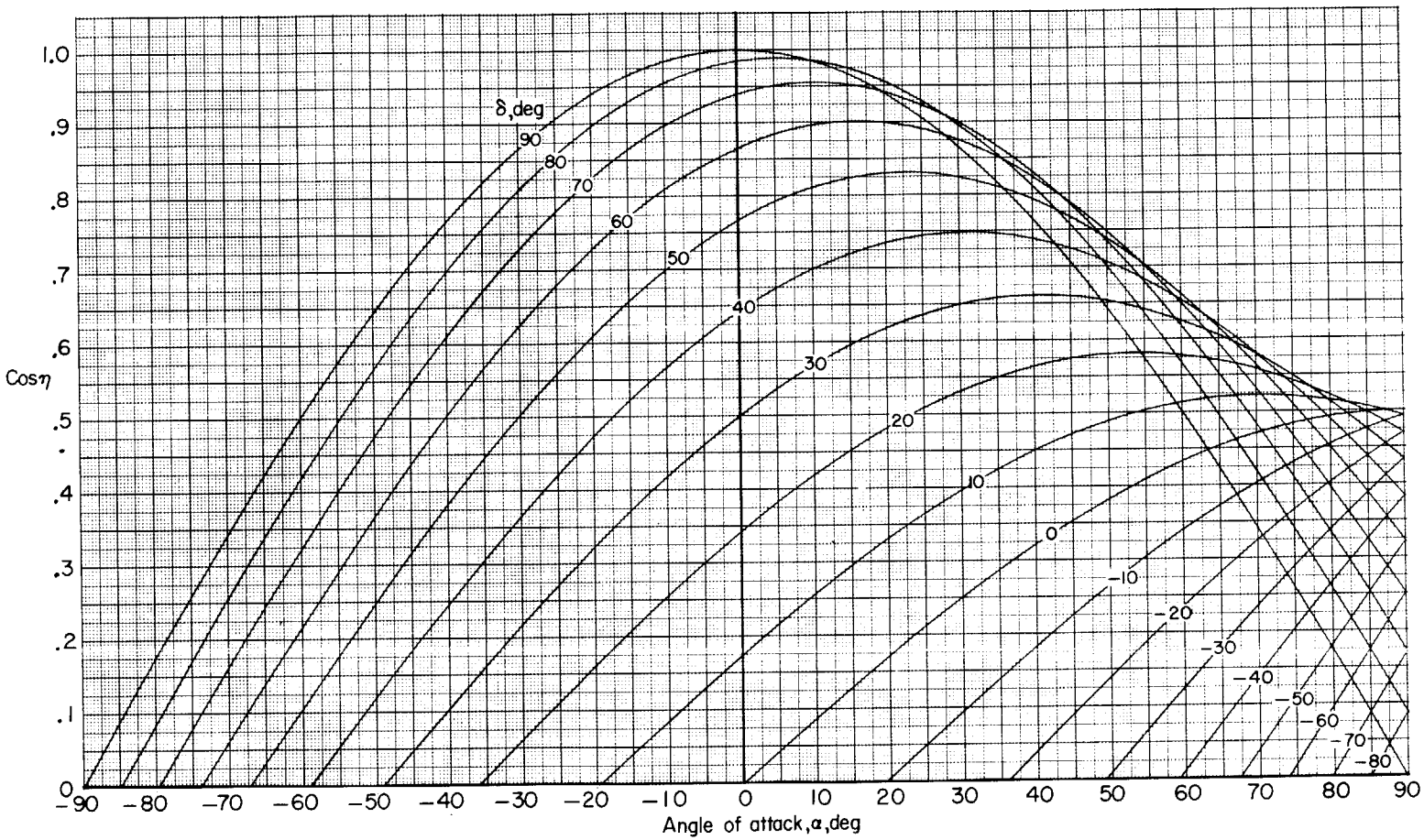

(g) $\Gamma = \pm 60^{\circ}$.

Figure 4.- Continued.

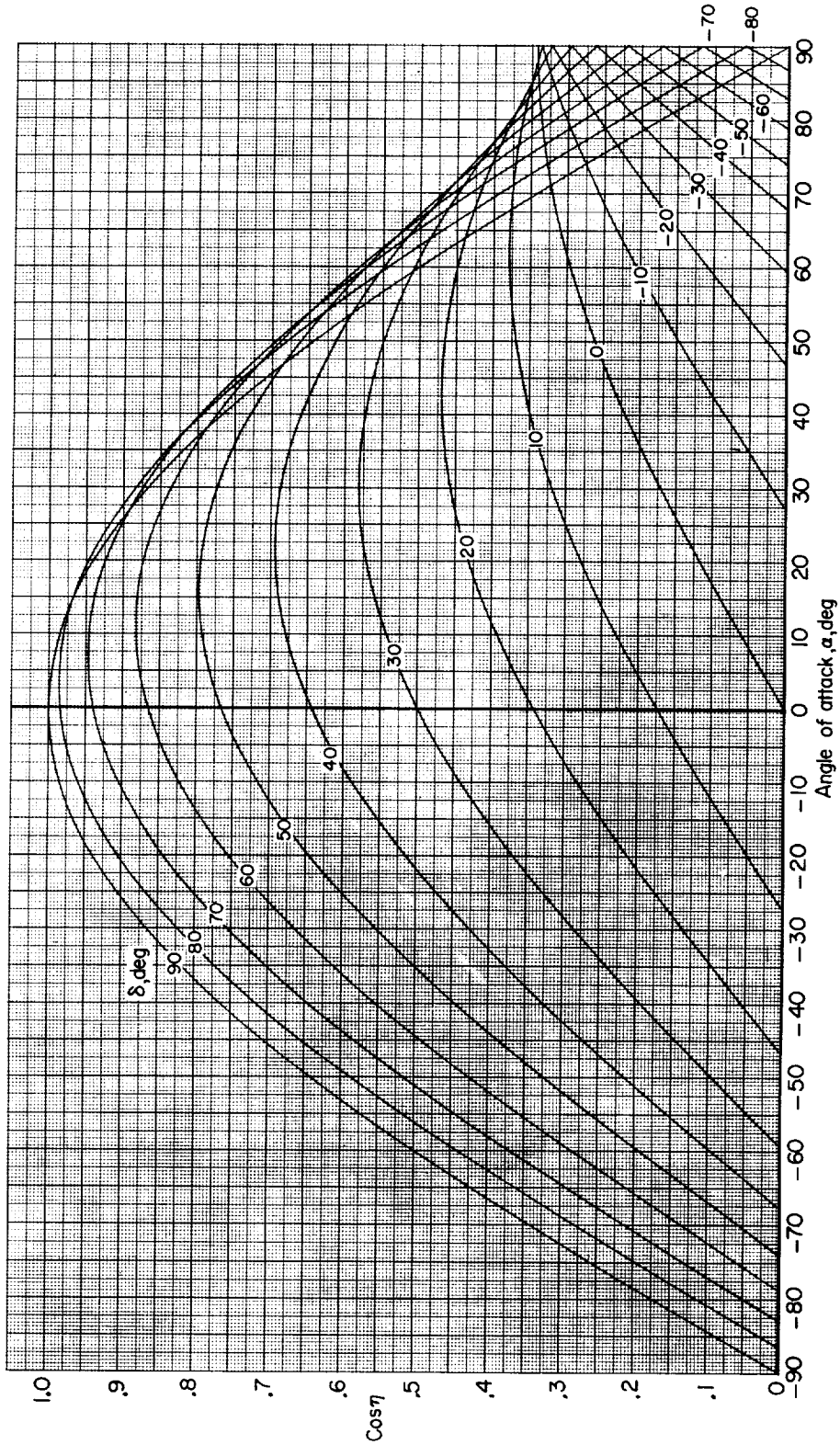

(h) $\Gamma = \pm 70^{\circ}$.

Figure 4.- Continued.

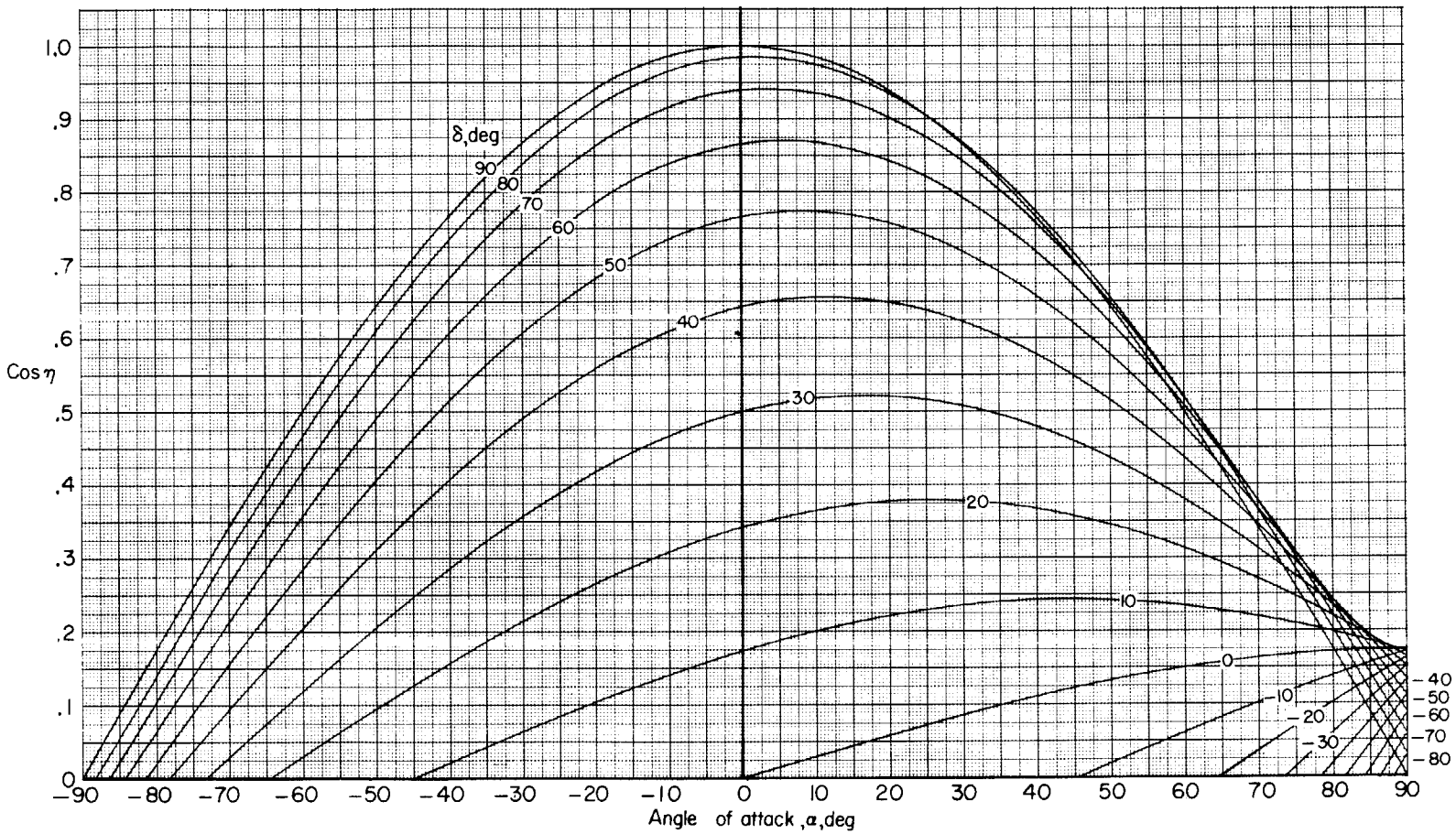

(i) $\Gamma = \pm 80^{\circ}$.

Figure 4.- Continued.

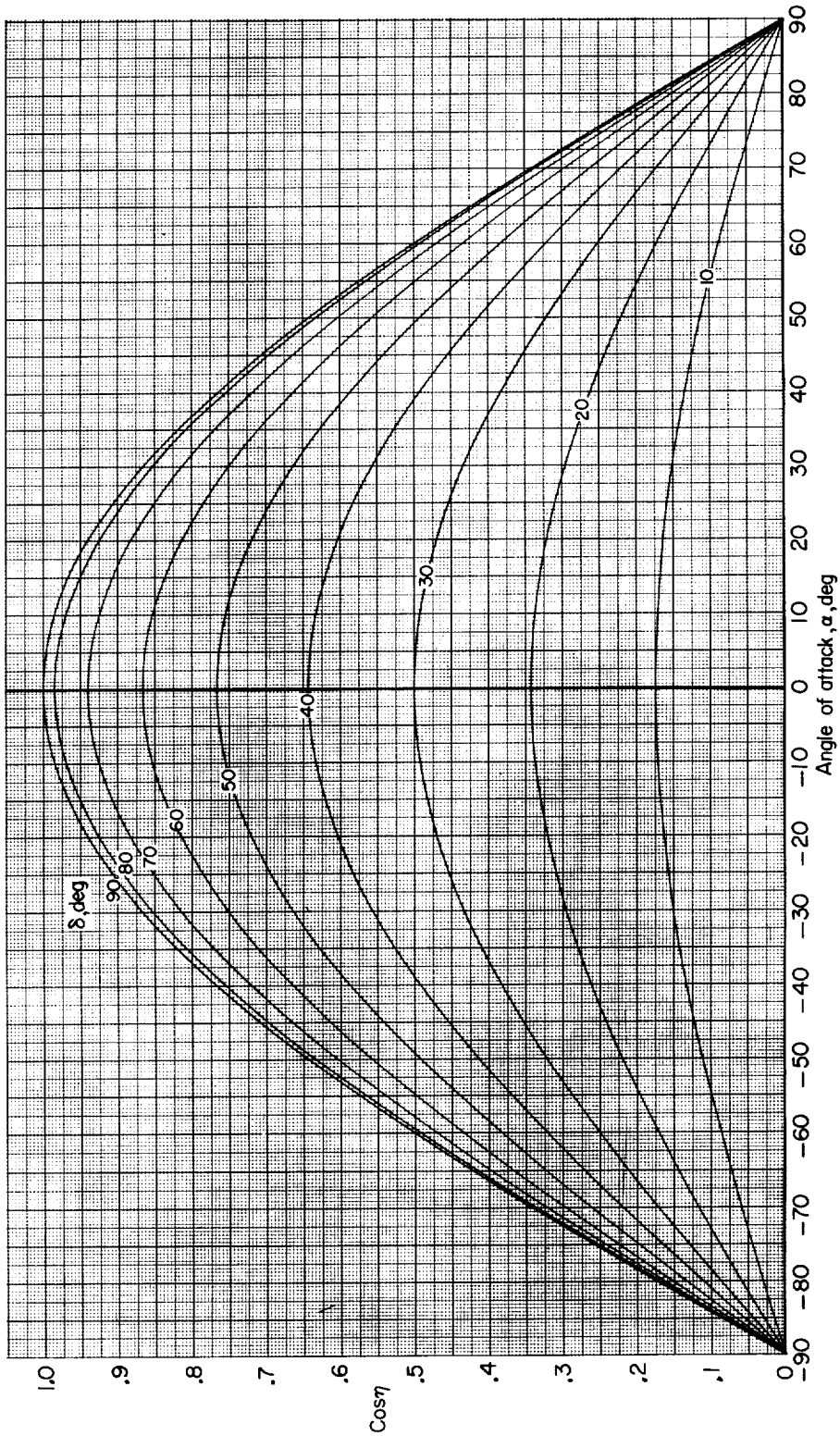

(j) $\Gamma = \pm 90^{\circ}$.

Figure 4.- Concluded.

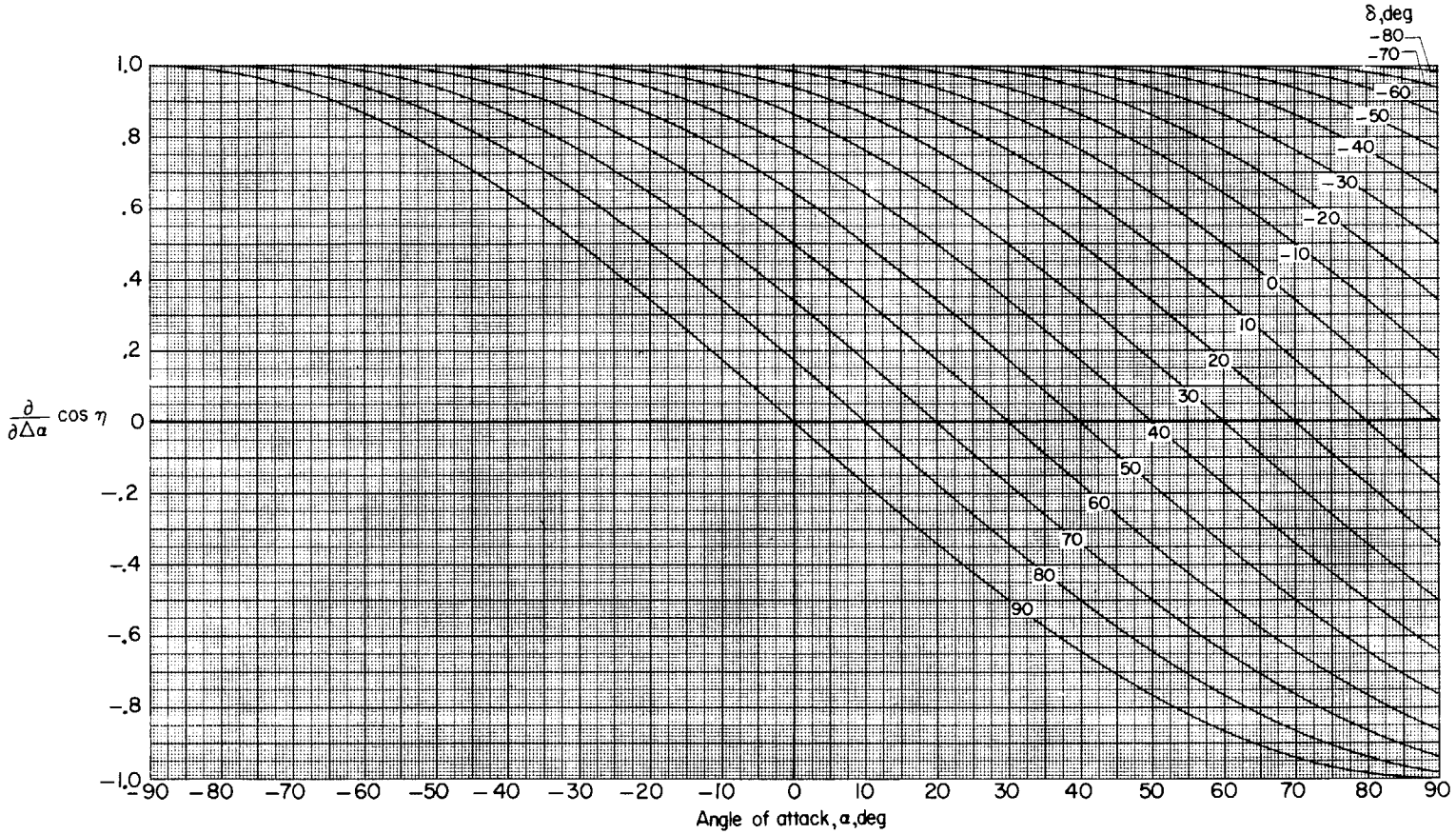

(a) $\Gamma = 0^\circ$.

Figure 5.- Variation of the parameter $\frac{\partial}{\partial \Delta\alpha} \cos \eta$ with angle of attack for various values of the surface orientation angles Γ and δ. $\beta = 0^\circ$.

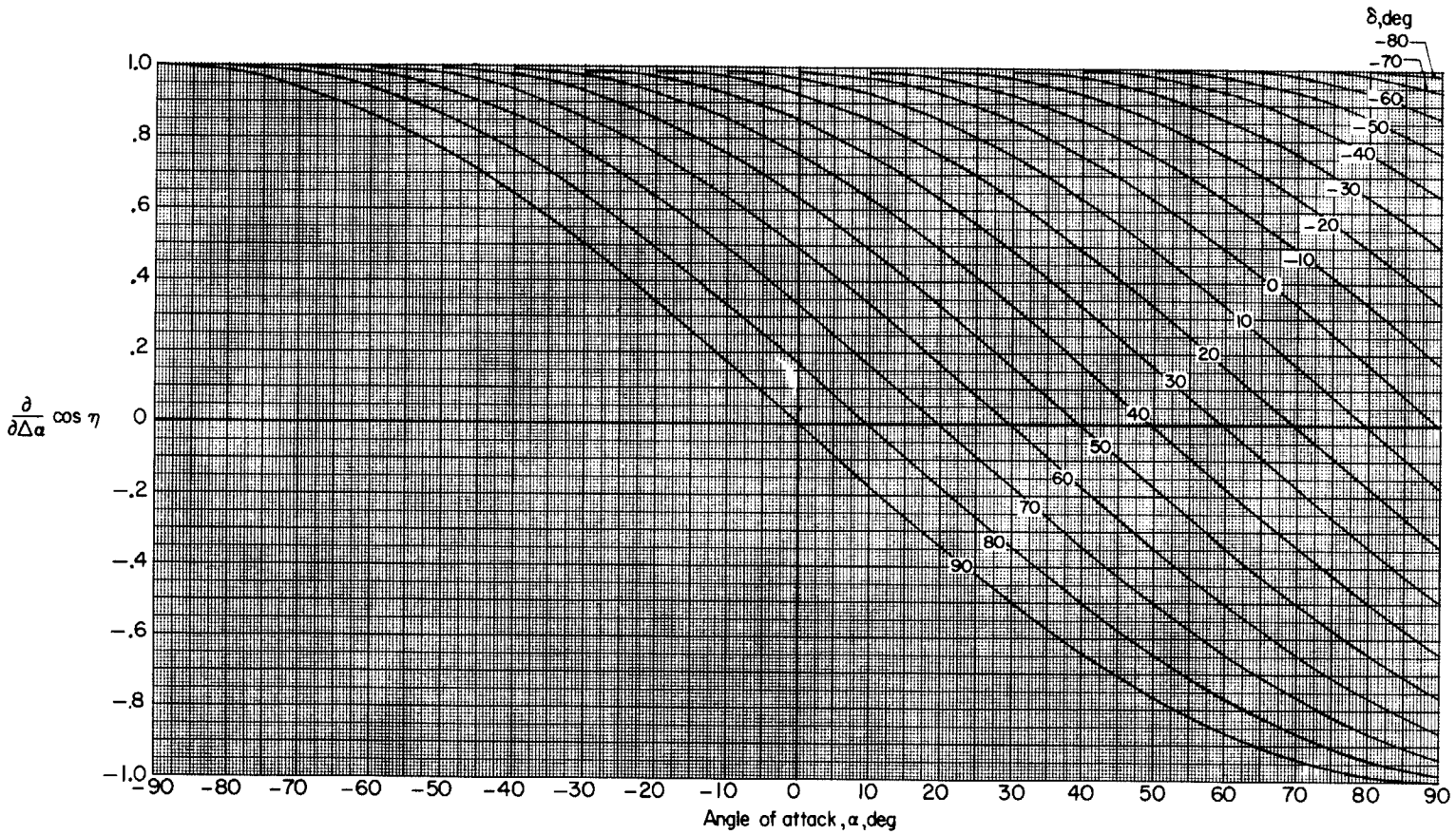

(b) $\Gamma = \pm 10^{\circ}$.

Figure 5.- Continued.

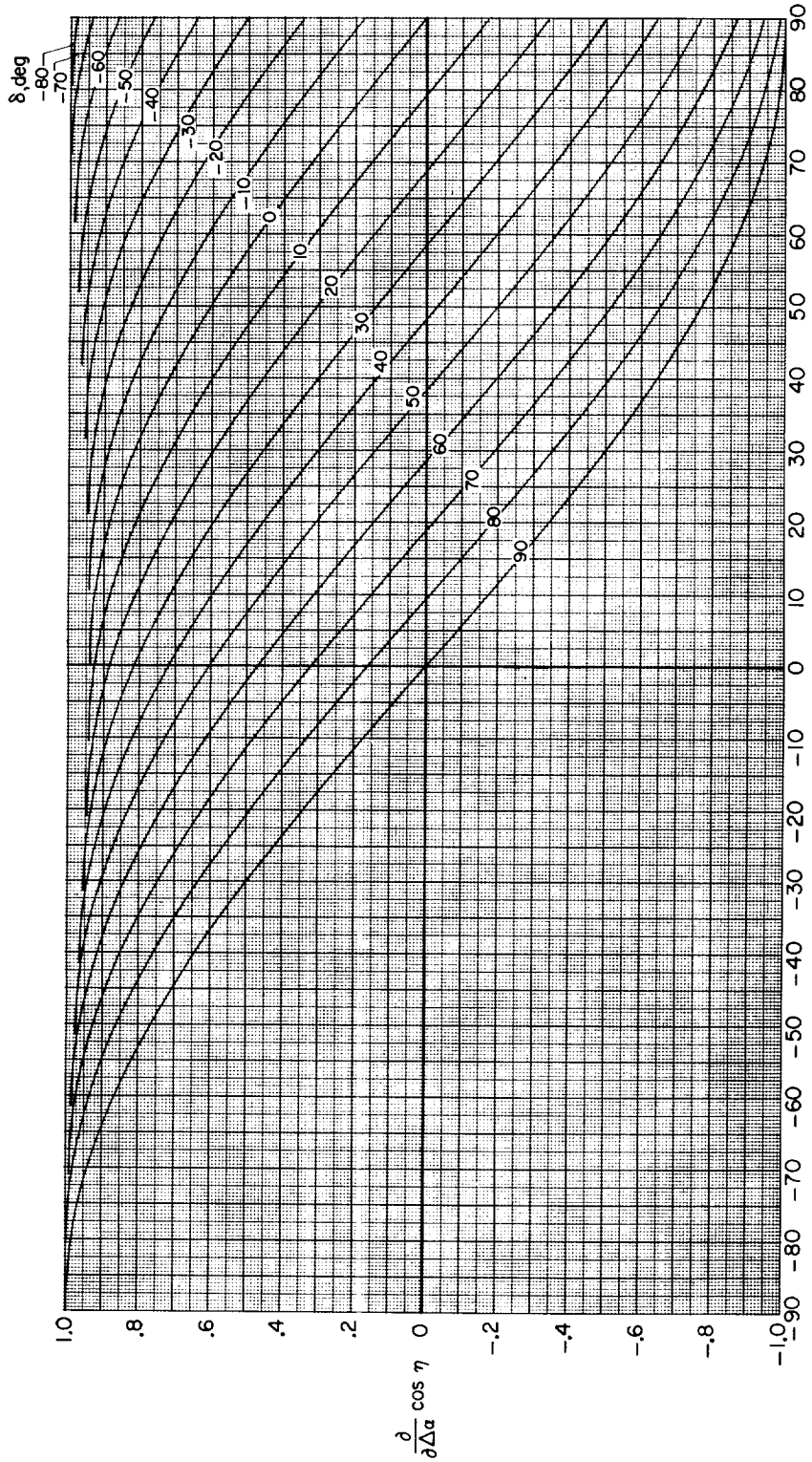

(c) $\Gamma = \pm 20°$.

Figure 5.- Continued.

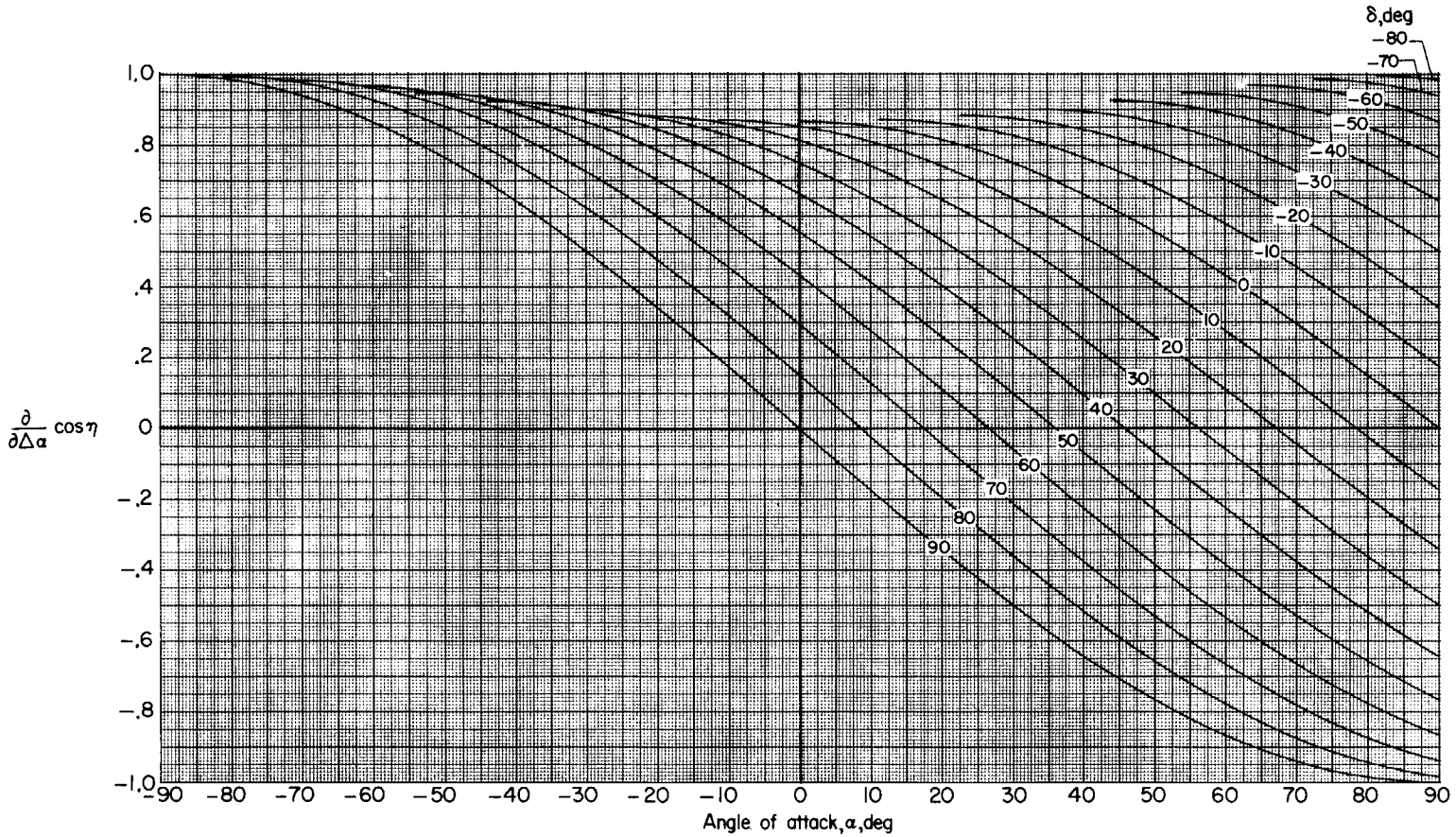

(d) $\Gamma = \pm 30^{\circ}$.

Figure 5.- Continued.

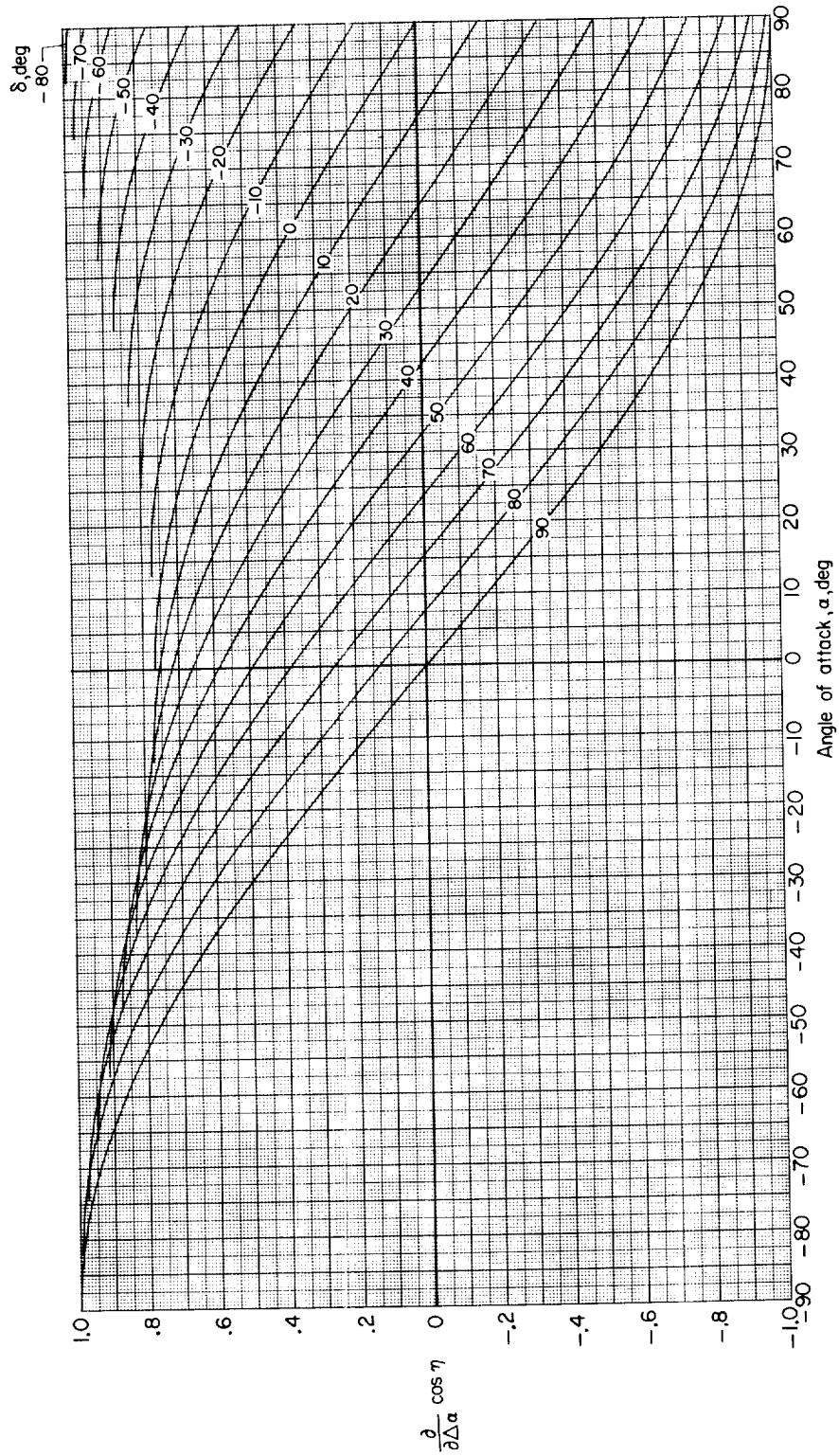

(e) $\Gamma = \pm 40^{\circ}$.

Figure 5.- Continued.

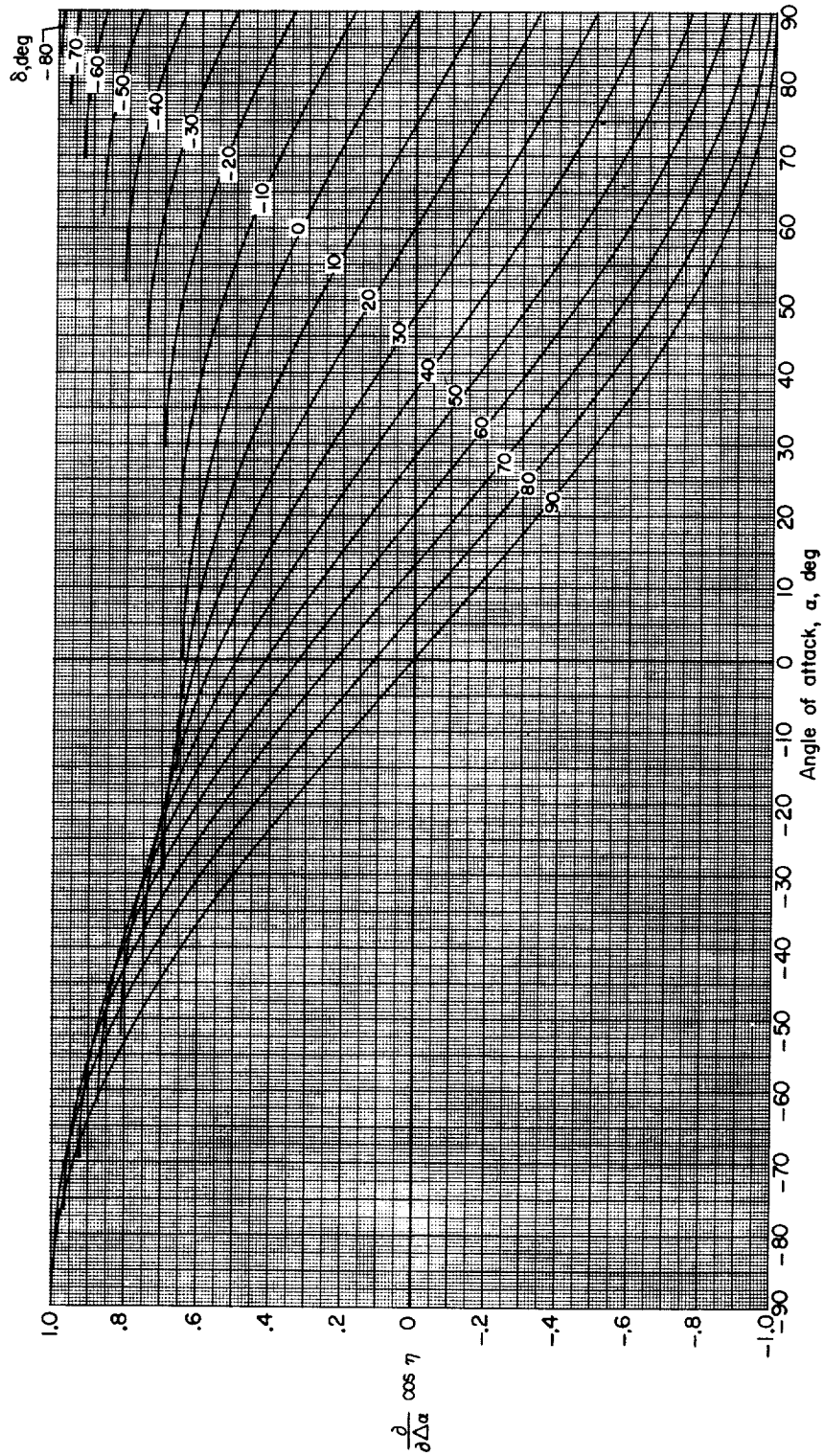

(f) $\Gamma = \pm 50^{\circ}$.

Figure 5.- Continued.

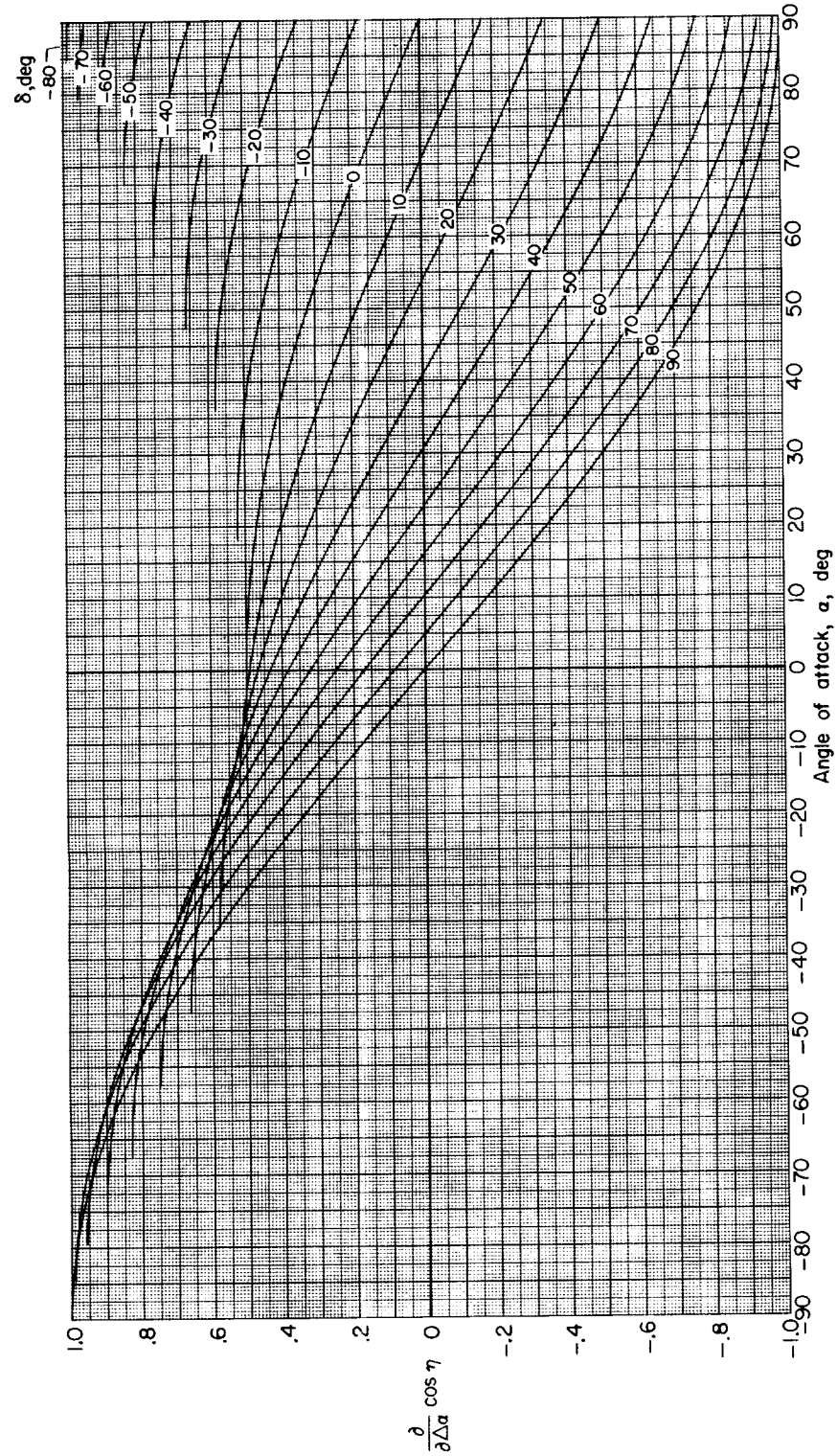

(g) $\Gamma = \pm 60^{\circ}$.

Figure 5.- Continued.

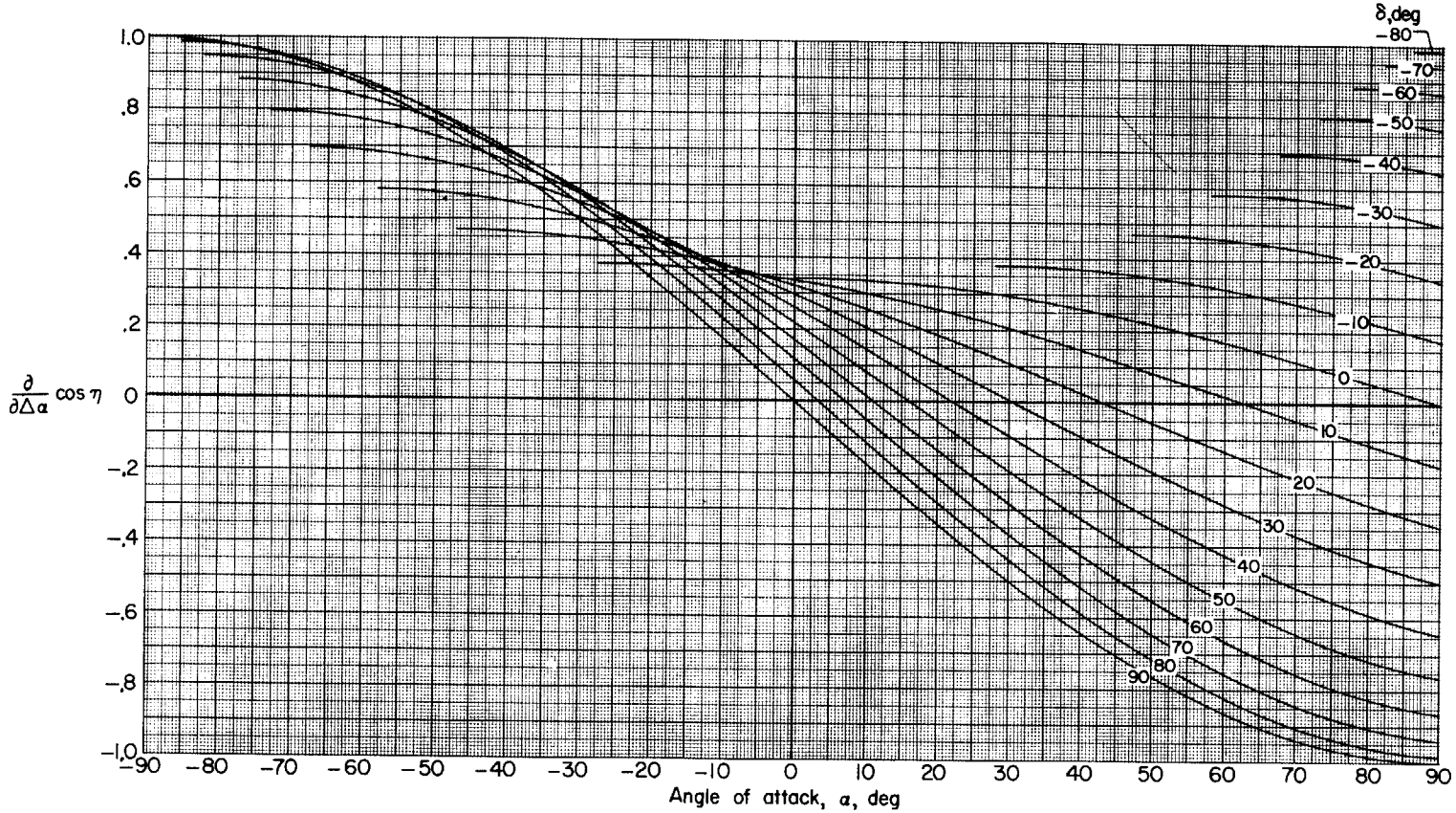

(h) $\Gamma = \pm 70^{\circ}$.

Figure 5.- Continued.

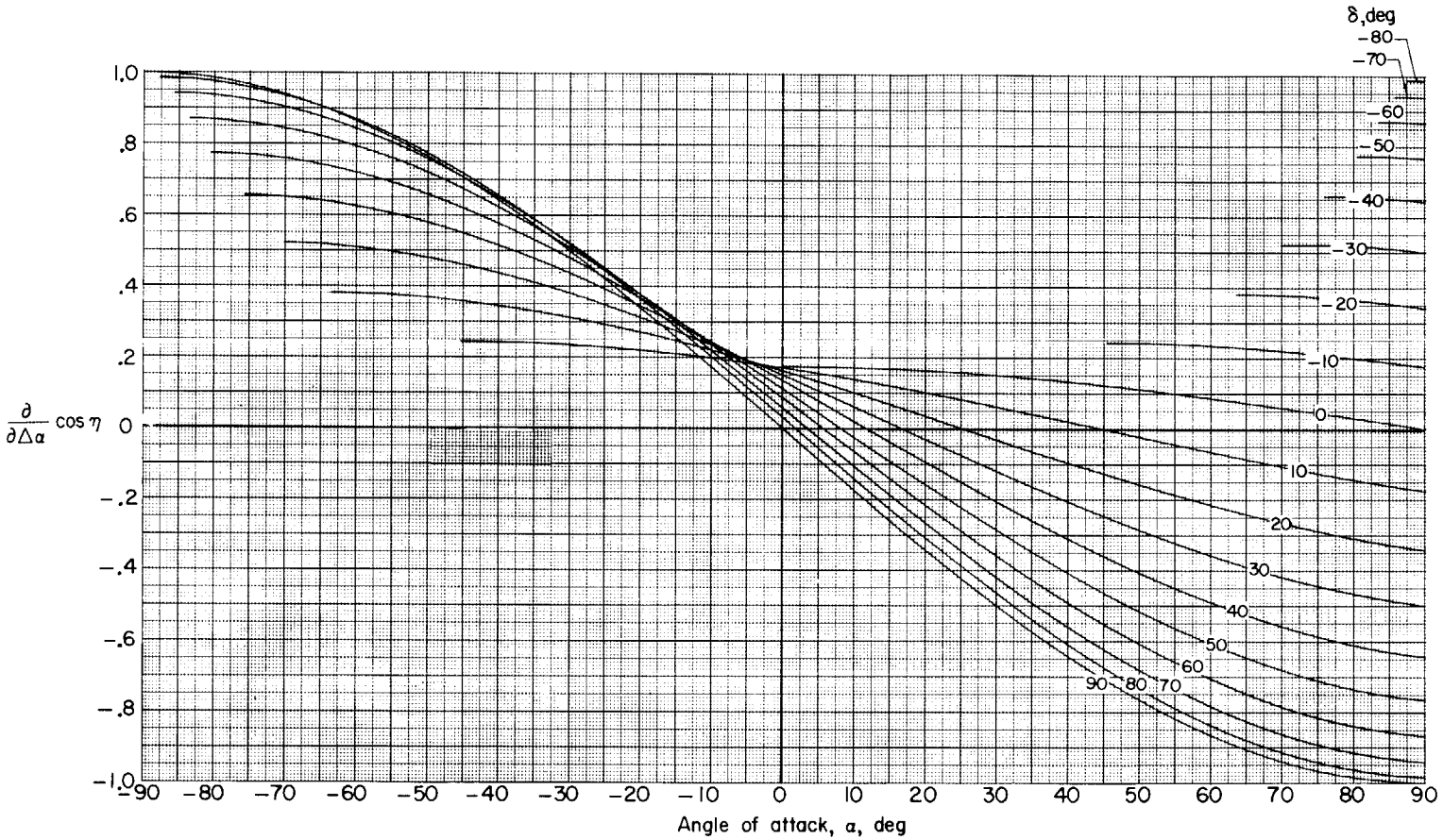

(i) $\Gamma = \pm 80^{\circ}$.

Figure 5.- Continued.

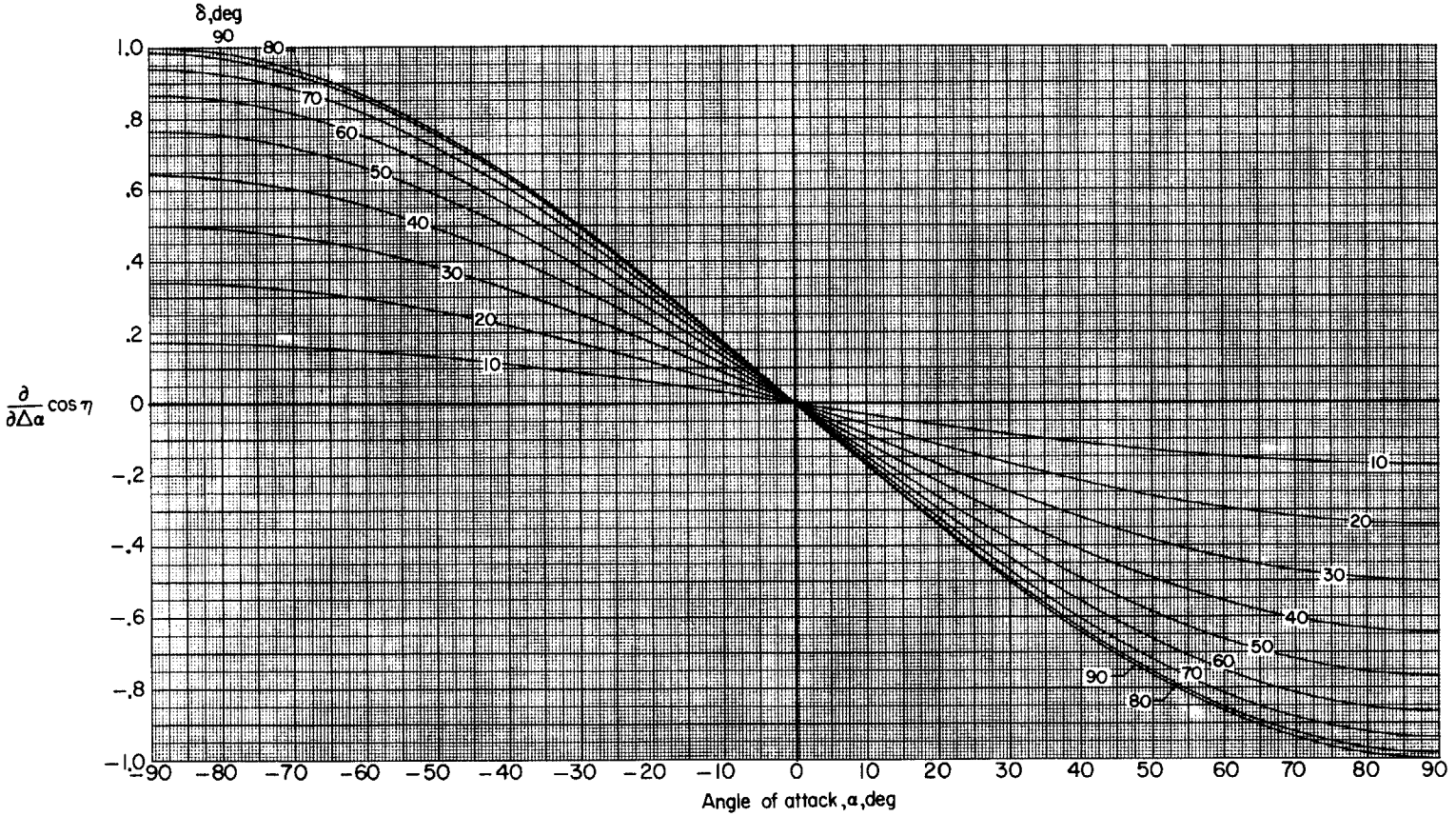

(j) $\Gamma = \pm 90^{\circ}$.

Figure 5.- Concluded.

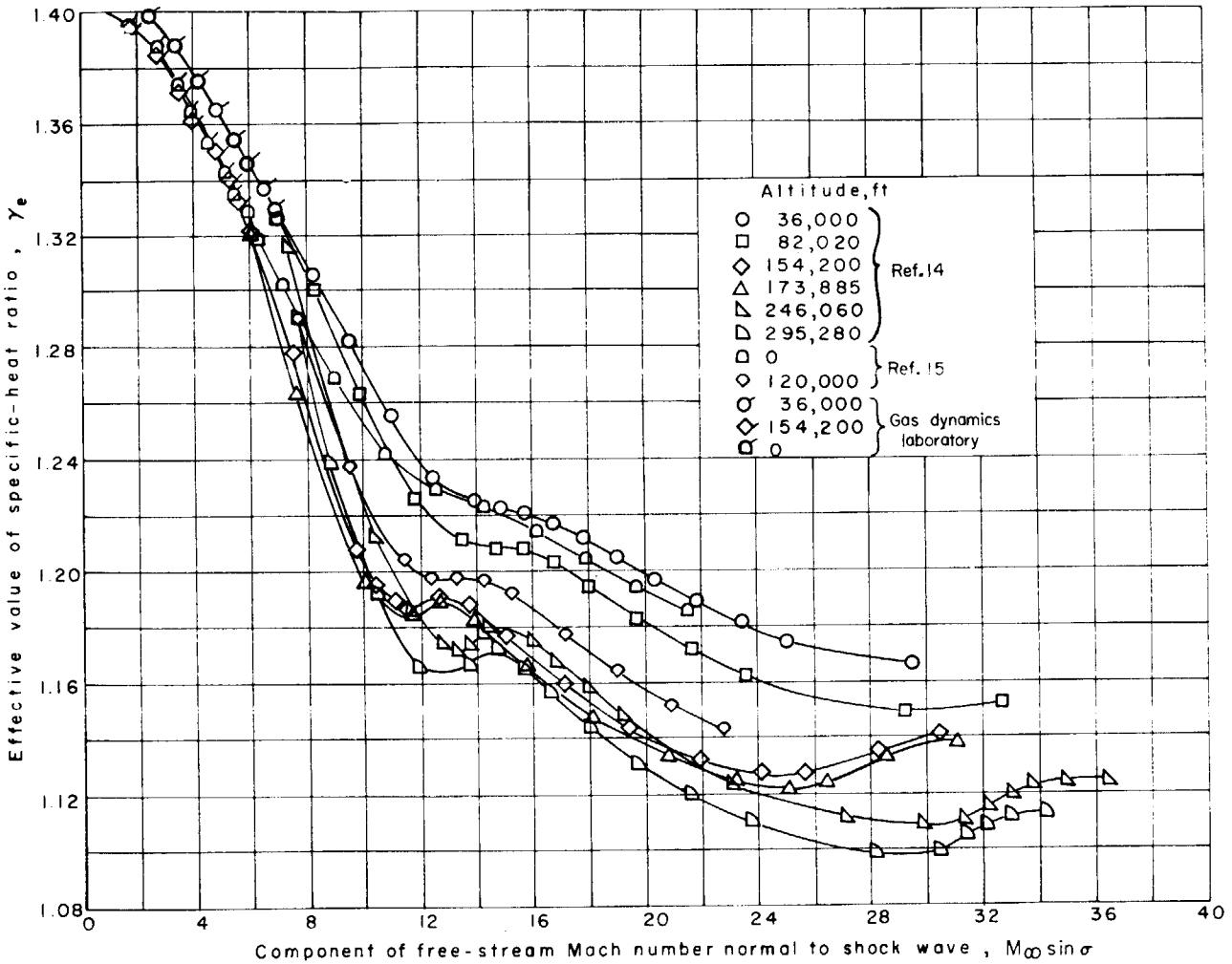

Figure 6.- Basic plot of γ_e against $M_\infty \sin\sigma$ for various altitudes. An argon-free atmosphere is assumed ($\gamma_\infty = 1.40$). (From ref. 12.)

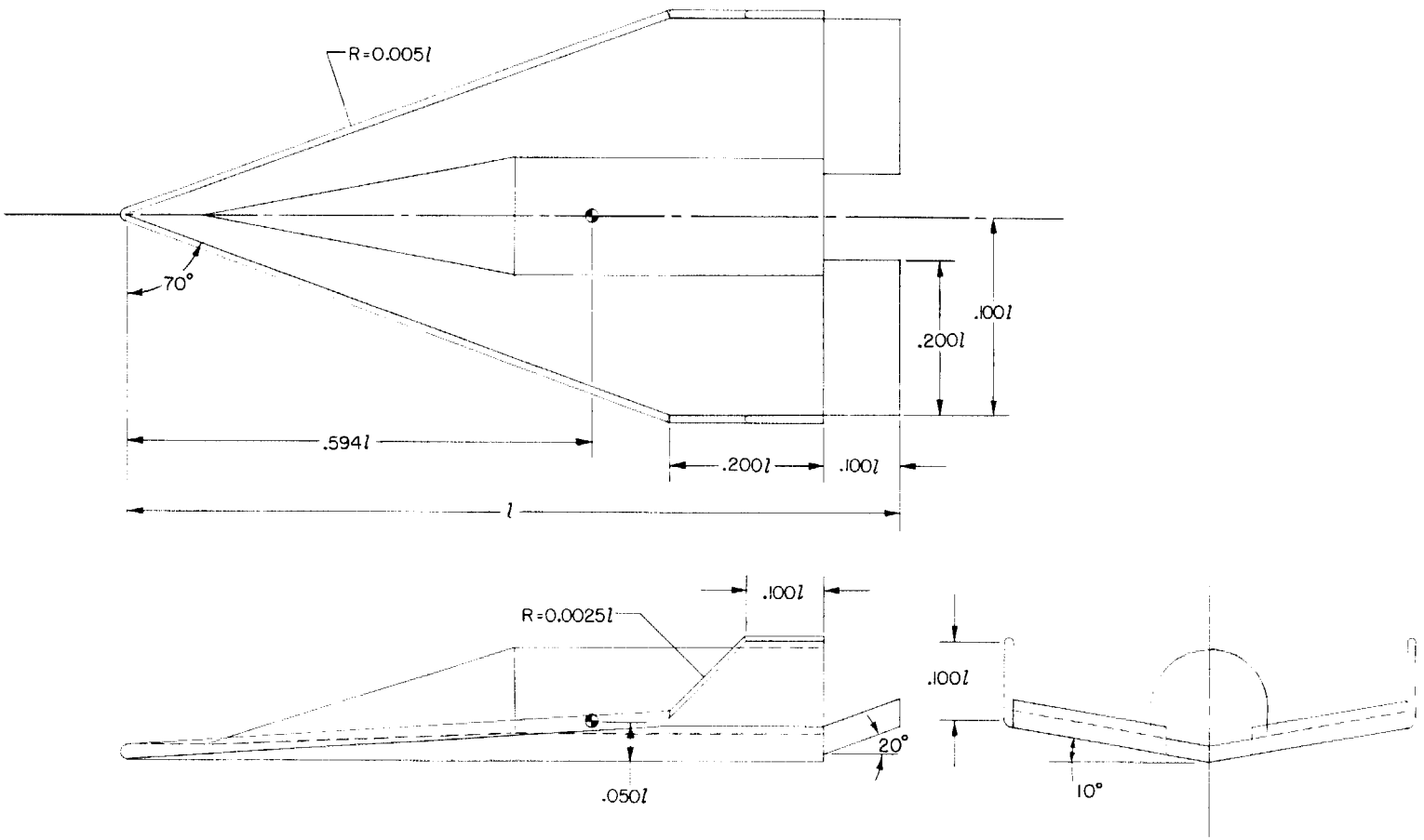

Figure 7.- Configuration studied in sample calculation. Dimensions shown are the dimensions of the undeflected planforms of the various surfaces.

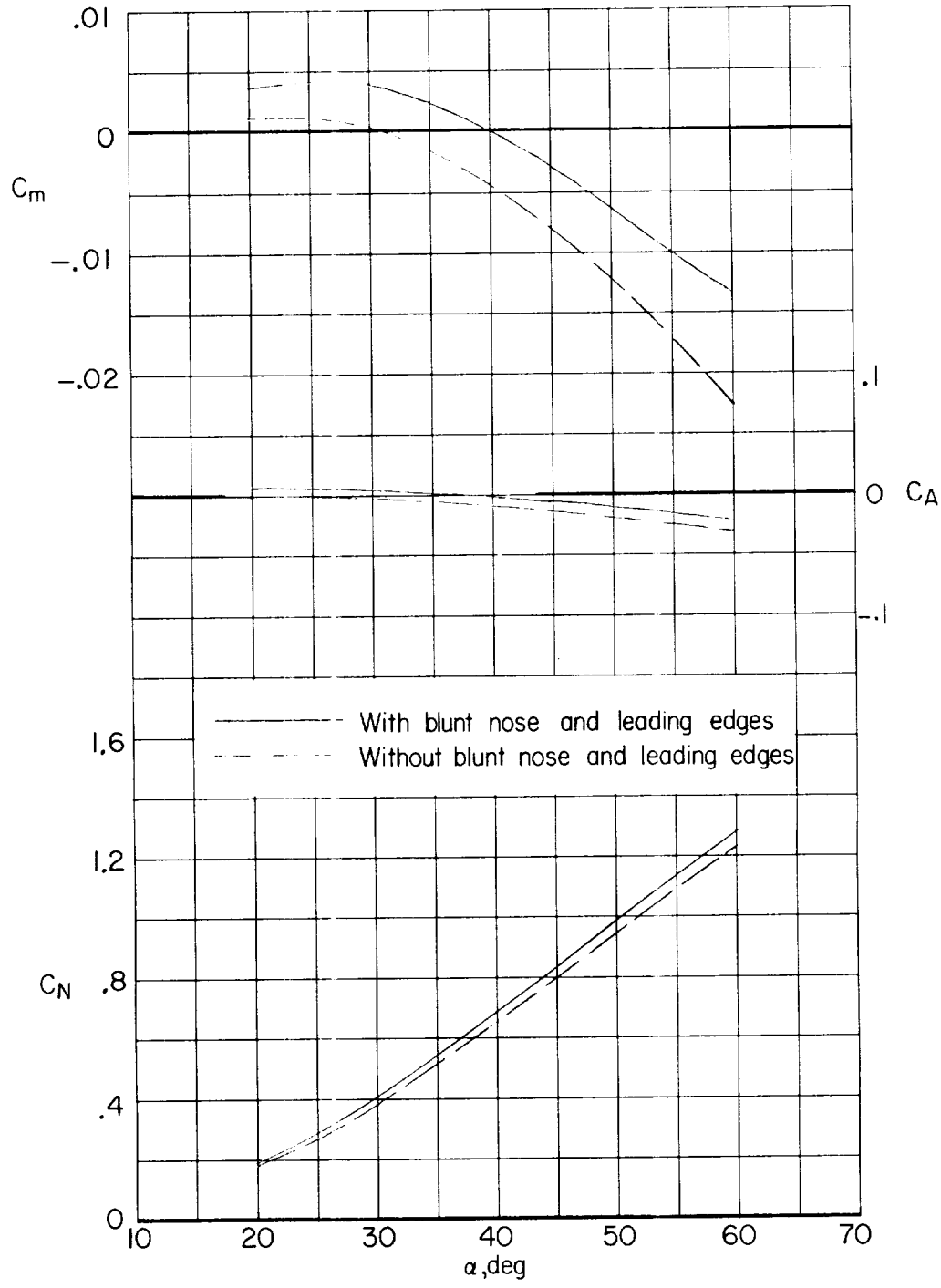

Figure 8.- Calculated aerodynamic characteristics of configuration shown in figure 7.

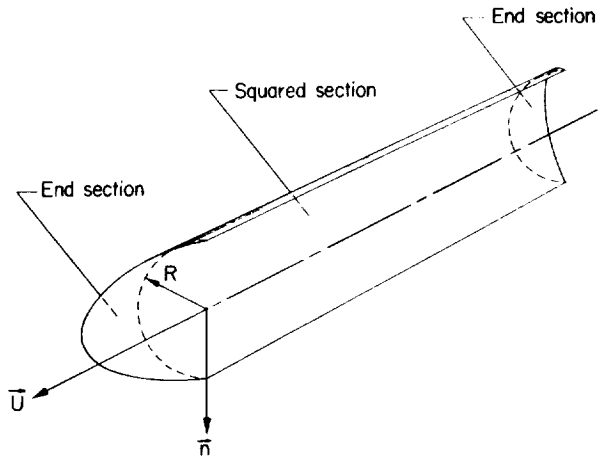

(a) Sketch of a hemicylindrical leading edge.

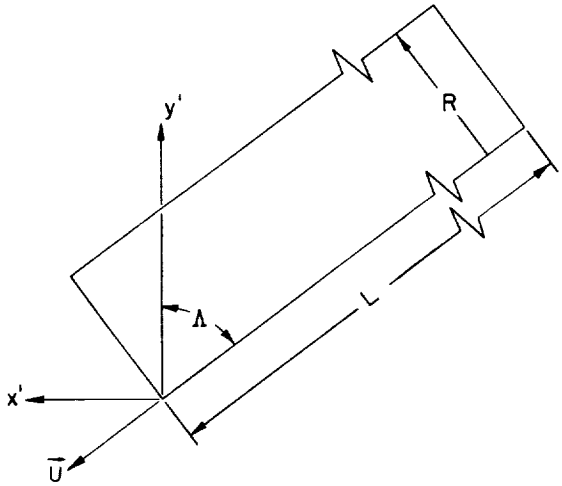

(b) Sketch showing square-cut section of hemicylindrical leading edge.

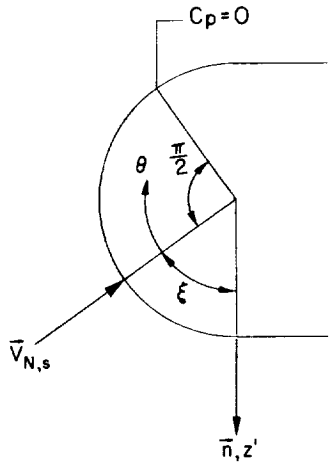

(c) Hemicylindrical leading edge cut by a plane normal to the leading-edge vector $\vec{U}$.

Figure 9.- Geometry of hemicylindrical leading edge.

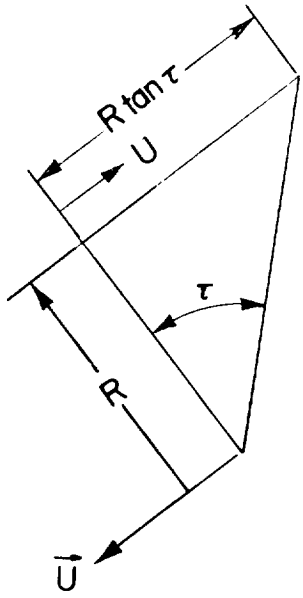

(d) End section of hemicylindrical leading edge.

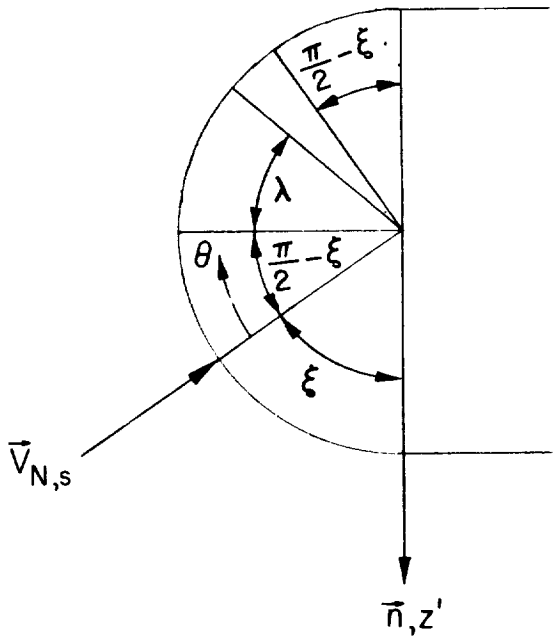

(e) Sketch in plane normal to the leading-edge vector $\vec{U}$ of end section of hemicylindrical leading edge.

Figure 9.- Concluded.

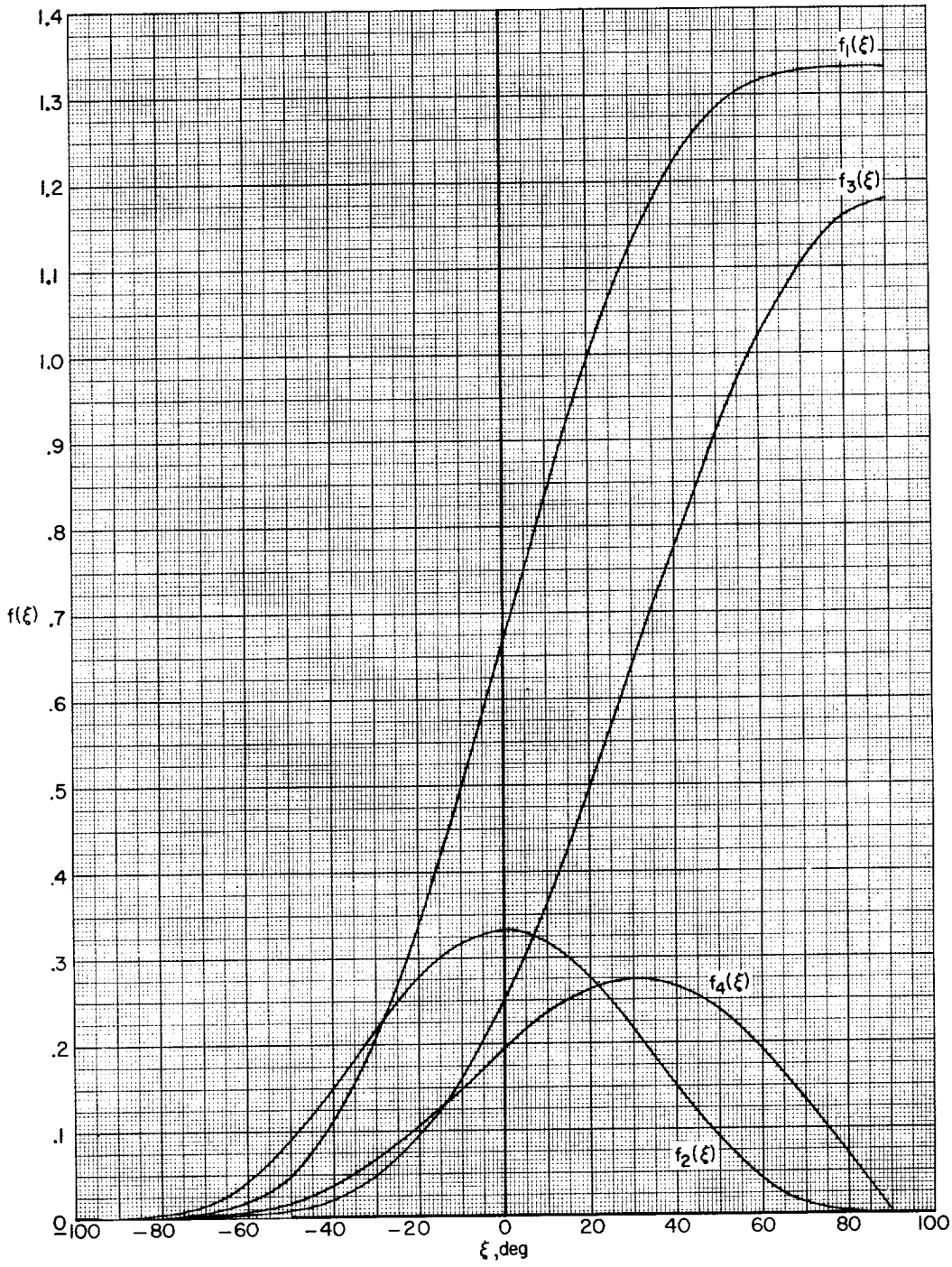

Figure 10.- Functions for the evaluation of aerodynamic force coefficients on hemicylindrical leading edges.

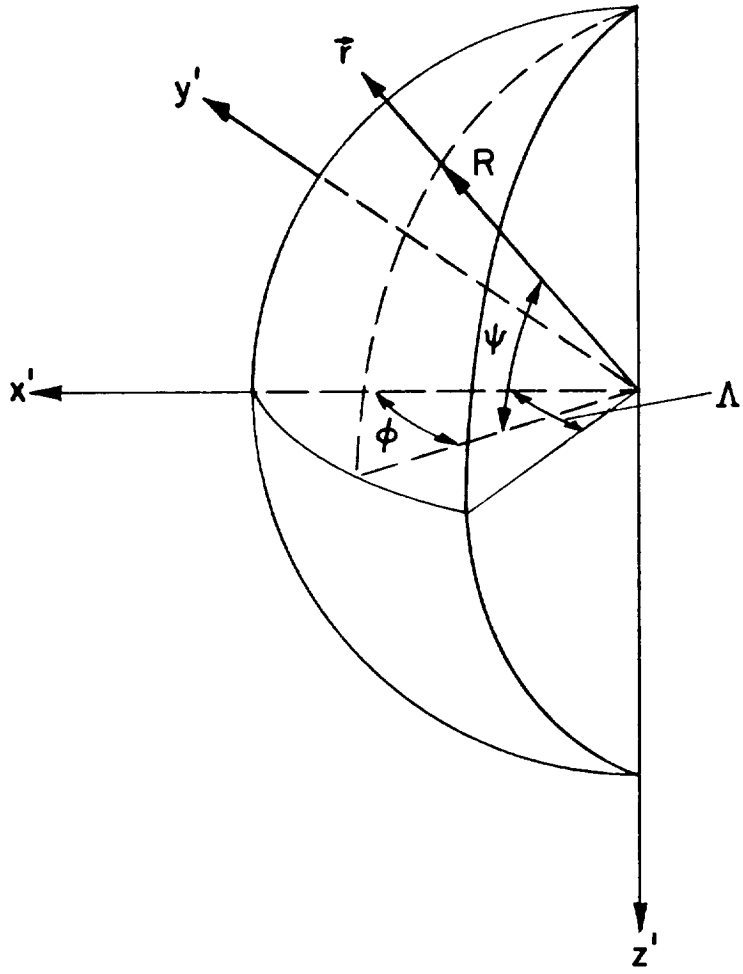

Figure 11.- Geometry of spherical-wedge nose section.

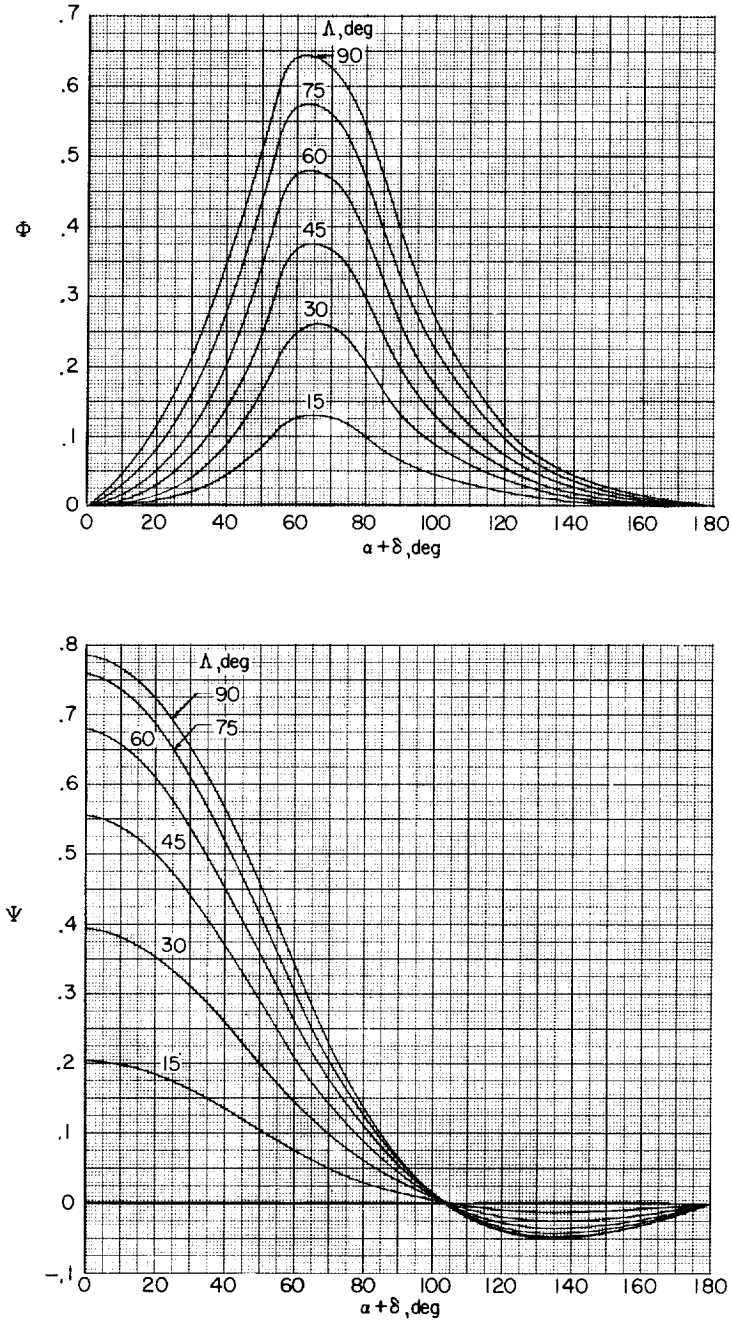

Figure 12.- Functions for determining the normal-force and axial-force coefficients on a spherical-wedge nose. $C_N = \frac{2K}{\pi}(\Phi \cos \delta - \Psi \sin \delta)$; $C_A = \frac{2K}{\pi}(\Phi \sin \delta + \Psi \cos \delta)$.